Biochimica et Biophysica Acta 1834 (2013) 1722–1738

Contents lists available at SciVerse ScienceDirect

Biochimica et Biophysica Acta

journal homepage: www.elsevier.com/locate/bbapap

Small ligand–globin interactions: Reviewing lessons derived from computer simulation ☆

Luciana Capece [a,b,1], Leonardo Boechi [c,1], Laura L. Perissinotti [d], Pau Arroyo-Mañez [a,e], Damián E. Bikiel [a], Giulietta Smulevich [f], Marcelo A. Marti [a,b,**], Dario A. Estrin [a,*]

[a] Departamento de Química Inorgánica, Analítica, y Química Física/INQUIMAE-CONICET, Facultad de Ciencias Exactas y Naturales, Universidad de Buenos Aires. Ciudad Universitaria, Pabellon 2, C1428EHA Buenos Aires, Argentina
[b] Departamento de Química Biológica, Facultad de Ciencias Exactas y Naturales, Universidad de Buenos Aires. Ciudad Universitaria, Pabellon 2, C1428EHA Buenos Aires, Argentina
[c] Department of Chemistry and Biochemistry, University of California San Diego, 92093 — La Joya, CA United States
[d] Institute for Biocomplexity and Informatics, Department of Biological Sciences, University of Calgary, 2500 University Dr. NW Calgary, Alberta T2N1N4, Canada
[e] Departamento de Química Orgánica, Facultad de Ciencias Exactas y Naturales, Universidad de Buenos Aires, Ciudad Universitaria, Pabellon 2, C1428EHA Buenos Aires, Argentina
[f] Dipartimento di Chimica "Ugo Schiff", Università di Firenze, Via della Lastruccia 3-13, I-50019 Sesto Fiorentino (FI), Italy

ARTICLE INFO

Article history:
Received 28 December 2012
Received in revised form 22 February 2013
Accepted 26 February 2013
Available online 5 March 2013

Keywords:
Computer simulation
Molecular dynamics
Heme protein
Globin
QM/MM

ABSTRACT

In this work we review the application of classical and quantum-mechanical atomistic computer simulation tools to the investigation of small ligand interaction with globins. In the first part, studies of ligand migration, with its connection to kinetic association rate constants (k_{on}), are presented. In the second part, we review studies for a variety of ligands such as O_2, NO, CO, HS^-, F^-, and NO_2^- showing how the heme structure, proximal effects, and the interactions with the distal amino acids can modulate protein–ligand binding. The review presents mainly results derived from our previous works on the subject, in the context of other theoretical and experimental studies performed by others. The variety and extent of the presented data yield a clear example of how computer simulation tools have, in the last decade, contributed to our deeper understanding of small ligand interactions with globins. This article is part of a Special Issue entitled: Oxygen Binding and Sensing Proteins.

© 2013 Elsevier B.V. All rights reserved.

1. Introduction

Globins are a superfamily of proteins with a particular globular fold, containing a heme moiety as a prosthetic group [1,2]. The archetypical cases are vertebrate hemoglobin (Hb) and myoglobin (Mb), displaying the classical 3-over-3 helical globin fold shown in Fig. 1. This fold is composed of helices A, B, E, F, G, and H plus the CD loop or region, which is a highly mutable segment, usually composed of two small C and D helices, with a flexible and variably long loop in between. Notably, the D helix is sometimes completely missing, like in the archetypical case of Hb alpha-subunits, or in the majority of both symbiotic and non-symbiotic plant hemoglobins. In recent years other important members of the globin superfamily, such as neuroglobin and cytoglobin, with similar folds, have been discovered in many organisms [3]. About a decade ago an entirely novel branch of the globin superfamily, called the truncated (trHb) or bacterial hemoglobins, was discovered in a widespread variety of organisms, including protozoa and plants. The distinguishing characteristic of the trHbs is their shortened edition of the globin fold, a 2-over-2 helical fold, due to the total or partial truncation of helix-A, and vestigial helix-F [4]. trHbs have been further divided, on the basis of phylogenetic analysis, into three groups, indicated as Groups I–III or identified with the letters N, O, and P, respectively [5]. Interestingly, the globin fold can also be enlarged, yielding bigger globins with additional helices, like in the archaea protoglobin [6]. The structural core, where the heme is located, is well conserved, and, thus, a topological notation can be used to identify a given residue across the whole globin superfamily.

The heme moiety and its local environment comprise the globin active site. The heme iron is coordinated to the four equatorial nitrogen atoms of the protoporphyrin. All globins have a conserved histidine located at position F8 (HisF8) (proximal ligand) that defines the so-called proximal site. In the sixth coordination position, the distal site, where most of the exogenous ligands bind, a water molecule is generally bound to the heme iron. The amino acids located in the vicinity of the heme on the distal site are referred to as the distal

☆ This article is part of a Special Issue entitled: Oxygen Binding and Sensing Proteins.

* Corresponding author at: Departamento de Química Inorgánica, Analítica, y Química Física/INQUIMAE-CONICET, Facultad de Ciencias Exactas y Naturales, Universidad de Buenos Aires. Ciudad Universitaria, Pabellon 2, C1428EHA, Buenos Aires, Argentina.
** Corresponding author.
E-mail addresses: marcelo@qi.fcen.uba.ar (M.A. Marti), dario@qi.fcen.uba.ar (D.A. Estrin).

[1] These authors contributed equally to this work.

1570-9639/$ – see front matter © 2013 Elsevier B.V. All rights reserved.
http://dx.doi.org/10.1016/j.bbapap.2013.02.038

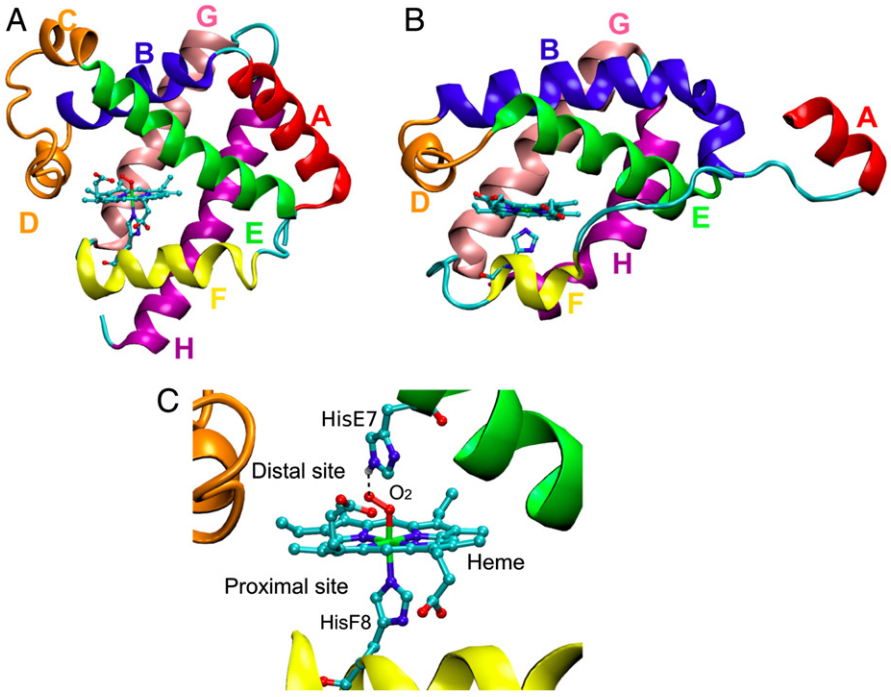

Fig. 1. A) Archetypical globin structure (that of Mb) depicting the typical 3-over-3 helical fold [7] (PDBid 2MGM). B) Truncated hemoglobin N of *M. tuberculosis* depicting the typical 2-over-2 helical fold [8] (PDBid 1IDR). C) Globins heme active site showing typical distal and proximal sites. (In C) the O_2-bound complex is shown as example.)

amino acids. (Fig. 1C) In vertebrate globins the typical distal amino acid is a histidine located at the E7 position (HisE7), but any other type of residue can be also found.

Due to the ubiquity and relevance of globins for the biological and biophysical sciences, over the decades, they have been the subject of numerous computational studies (see references [9–14] for reviews on the subject). Moreover, given that Mb was the first protein to be crystallized and the model of choice for developing many spectroscopic and other biophysical methods, there is a wealth of detailed information that can be directly related to simulation-derived results, thus providing a stringent test for the accuracy and predictive power of theoretical methods [12,15–21]. The heme itself has interesting chemical properties, which rely on its peculiar electronic structure and have also been the subject of many theoretical studies [22,23]. Last but not least, hemoglobin is the hallmark of an allosteric protein, and thus many simulation-based works have been performed to understand its mechanism and characteristics [24–27].

The function of globins is in many cases still a matter of debate, but it is generally accepted that their reactivity towards small ligands, such as O_2, NO, CO, HS^- and NO_2^- among others, plays a key role [28,29]. The affinity for certain ligands is determined by several factors, including the intrinsic reactivity of the ligand for the heme. This reactivity is further modulated by both the proximal residues [30], which can fine tune the heme electronic structure, and the distal residues that may interact directly with the bound ligand [9,31,32]. Furthermore, the reactivity depends on the ligand accessibility to the distal site, which can be modulated by the presence of i) blocking residues that coordinate to the iron, ii) tunnels connecting the distal site with the solvent [8,33], and iii) gates that may dynamically control access and escape routes [34]. The dynamics of the active site residues may also play an important role in both small ligand affinity and reactivity [9].

The ligand affinity is characterized by the equilibrium constant K_{eq}, defined by the ratio between the kinetic rate constants of the ligand association and dissociation processes, k_{on} and k_{off}, respectively [34]. From a microscopic viewpoint the association process can be divided in two elementary steps, ligand migration (or entry) from the solvent to the distal site, and formation of the iron–ligand bond. Diatomic hydrophobic ligands such as CO, NO or O_2 have similar ligand migration rates, but different bond formation rates. This is mainly determined by the inherent chemical reactivity of the ligand and can be understood in terms of both the electronic states of the reactant, and the position of the iron in the heme group [35]. As a result, there is a correlation between the ligand type and its association rate constant, which typically follows the following trend: k_{on} NO > k_{on} CO > k_{on} O_2 for the same protein [36].

For markedly polar or charged ligands (HS^-, NO_2^-, CN^-), specific protein–ligand interactions may strongly modulate the association rate. In some cases, experimental values of the elementary rate constants for the entry (k_{entry}) and bond formation processes (k_{bond}) are available. The aforementioned processes can be studied using computer simulations. For ligand entry and escape, the ligand pathways can be determined using classical Molecular Dynamics (MD), and usually the free energy profile along the pathways can be measured using a combination of classical Molecular Dynamics (MD) with different enhanced sampling methods that we will describe in the next section [12,16,37,20,38–44]. On the other hand, studying the formation of iron–ligand bonds requires a quantum mechanical (QM) model, since significant changes in the electronic structure are involved [9,11,35].

The dissociation rates also depend on two main factors: the strength of the iron–ligand bond, and the protein–ligand interactions in the bound state. Given that the chemical nature of the ligands affects both properties, measured dissociation rates span a wide range of values, from 10^{-4} s^{-1}, for the Fe^{II}–NO adducts due to the very strong Fe–N bond, to 10^4 s^{-1} [34], for the weakly bound oxy complexes. In addition to the dissociation rates, a large amount of structural information is available. Crystal structures and resonance Raman spectroscopy studies of globins that bind to O_2, NO, CO, NO_2^-, among other ligands, are available [45–49]. MD simulations of the bound complexes are extensively used to study globin–ligand conformations and dynamics [11,12,50]. In addition, QM-based methods can be used to evaluate

the heme–ligand structure and the bond strength, and thus correlate this information with the dissociation rate [9].

In the present review, we describe how computer simulation tools can shed light on the molecular basis that governs small ligand interactions with globins, by first revising the basic methodological ideas. We include a representative number of examples investigated in our group during the last decade, presented in the context of other groups' theoretical and experimental studies. The variety and extent of the presented data yield a clear example of how computer simulation tools have contributed to our deeper understanding of this widespread and complex process.

2. Computational methods

From a technical point of view, computational methods to study globins can be divided into two broad categories: (1) those that rely on quantum mechanics (QM), that are needed to understand heme reactivity and permit formation and breakage of the iron – ligand bond, and (2) those based on classical Molecular Dynamics (MD), used to study small ligand migration and globin conformational dynamics [50]. In the following sections we will describe how both types of methods can be used to study the interaction between globins and small ligands.

2.1. Quantum mechanical (QM) methods

QM-based methods, usually those based on density functional theory (DFT), are used whenever a detailed description of the electronic structure of the heme and its direct environment (i.e. proximal and distal ligands) is needed, or when chemical reactions (including formation/breakage of the iron – ligand bond) are involved [50]. Performing geometry optimizations of the core porphyrin, a proximal histidine-mimicking imidazole, and the bound small ligand (i.e. O_2, CO, NO etc.) *in vacuum* at the DFT level with a medium to large basis set (6–31G** or D/TZP), allows the determination of proper geometry, including the iron–ligand key geometrical parameters [50,51]. Obtaining accurate energetics, like determination of the heme – ligand bond energy (ΔE_{Heme-X}) is far more difficult, since this requires an accurate determination of the heme–ligand (E_{Heme-X}) and free heme (E_{Heme}) energy, as shown by Eq. (1):

$$\Delta E_{Heme-X} = E_{Heme-X} - (E_{Heme} + E_x) \quad (1)$$

where E_{Heme-x} is the energy of the heme–ligand complex, E_{Heme} is the energy of the ligand-free (i.e. pentacoordinated) heme and E_x is the energy of the ligand *in vacuum*. The main obstacle in obtaining accurate ΔE_{Heme-X} values lies in the fact that when the ligand binds, the heme may change its ground spin state. In the imidazole-bound pentacoordinated (5c) state, the ferrous heme displays a quintet ground state. In its hexacoordinated (6c) state, for example the oxygen-bound (oxy) heme, the CO adduct, and the ferric NO-bound heme, the heme often displays singlet ground states, and the ferrous NO-bound heme displays a doublet ground state. Other ferric 6c states, especially those formed with strong field ligands, like, F^-, CN^- and HS^-, also have low spin states, usually a doublet. Ferric H_2O- or OH^--bound states may display also intermediate or high states, depending on the protein. One of the limitations of DFT lies in describing spin gaps, often making binding energies that usually do not agree with experimental values, and highly dependent on the exchange correlation functional and basis used [22]. However, as will be shown in the examples below, the trends in binding energies obtained for different heme groups (or proteins) shows good correlation with the experimentally observed trends and can be used to state predictions [9].

2.2. QM/MM methods

A natural extension of the QM methods, which includes the electrostatic and steric effects of the surrounding protein on the heme structure and reactivity, is the use of the so-called hybrid QM/MM methods [52]. In the cases presented in this review, these methods are used to treat the protein active site, the heme and its ligands with a QM method as described above, and describe the rest of the protein environment using a classical (MM) force field. In many QM/MM schemes, like the code developed by our group (*Hybrid*) [53], the coupling between QM and MM subsystems is modeled through an additive Hamiltonian scheme, in which, the electronic density is computed and converged in a self-consistent field (SCF) scheme in the potential determined jointly by the QM-described atomic nuclei and MM-described fixed atomic partial charges. The electrostatic interaction between the QM electronic density and MM atomic partial charges is evaluated using Coulomb's law. An additional term describing the Van der Waals (vdw) and short-range repulsive interactions between all QM atoms MM atom pairs is included, usually through a Lennard–Jones potential [53]. Due to their high computational cost, QM/MM calculations are performed usually on selected snapshots extracted from MD trajectories, to obtain geometries and energy changes by optimization procedures.

2.3. Molecular mechanics (MM) methods

Molecular mechanics, or classical molecular dynamics, methods, are based on classical force fields and are the method of choice to study globin structural dynamics and its relation to the process of ligand migration pathways [12]. When starting the study of a given globin through MD simulations, one has to choose the starting structure and the force field. The starting structure is typically taken from the crystal structure of the protein.

2.3.1. Force field parameters

For a proper description of the different amino acids, many reliable force fields are available, [54] such as the Amber99 (SB), [55] or Charmm, [56] which are widely used for classical simulation studies of proteins. A critical point when performing MD simulations of globins are the parameters associated with the heme group and its ligands. Typically all bonded and Lennard–Jones parameters can be obtained from the force field general parameters. It is crucial, however, to very carefully assign the atomic charges, the equilibrium bond length and angle values for the ligand, since they are essential to obtain accurate results for each heme coordination/oxidation state. These parameters can be obtained from QM calculations of the corresponding porphyrin-ligand *in vacuum*, in combination with a charge fitting procedure, like the RESP method [57]. Usually, these charges, although obtained *in vacuum*, are used for all possible distal environments, those containing typical HisE7 as well as other cases like those of the TrHbs where TyrB10, TrpG8, GlnE7 and other residues can be found [9]. Nevertheless, it should be noted that these ligand charges may not be sufficiently accurate for all protein environments, and some adjustments may be needed, especially for ligands like O_2 and CO, as described in greater detail in the representative examples. For oxy-hemes, for example, a positive distal environment (defined by the presence of several hydrogen bond donor residues, like TyrB10 and TrpG8) increases the negative charge on the bound oxygen and should be considered to properly describe the active site dynamics. In the case of CO, a negative distal environment (where mostly hydrogen bond acceptors are found interacting with the ligand) favors a more neutral or even slightly positive charge on the oxygen atom.

For the charged ferric-bound strong field ligands (F^-, SH^- and CN^-), the ligand charge tends to depend less on the distal environments. In such cases the ligand interactions with the distal residues

Table 1
Bond and angle equilibrium values, and partial charges for the different heme-ligand complexes considered here. X and Y correspond to the ligand atoms, where X is the atom directly coordinated to the Fe and Y is bonded to X. Distances, angles and charges are given in Angstrom, degrees and *e*, respectively.

	Fe^{II}–O_2[a]	Fe^{II}–CO[b]	Fe^{II}–NO	Fe^{III}–NO	Fe^{III}–F^-	Fe^{III}–HS^-	Fe^{III}–NO_2^-[c]	Fe^{III}–ONO^-[c]	Fe^{III}–CN^-
qX	−0.l2	0.28	−0.03	0.40	−0.36	−0.19	0.37	0.44	0.16
qY	−0.18	−0.23	−0.04	0.20	–	0.09	−0.46	−0.55/−0.54	−0.46
d Fe-X	1.76	1.76	1.72	1.64	1.80	2.25	1.95	1.88	1.86
d X–Y	1.29	1.18	1.12	1.16	–	1.35	1.26	1.37/1.23	1.18
<Fe-X–Y	121	180	140	180	97	100	120	122	180
d Fe–HisF8	2.10	2.02	2.18	2.04	2.38	2.01	2.08	2.08	2.05
Reference	[11]	[11]	[11]	[11]	[58]	[59]	[60]	[60]	This work

[a] O_2 charges correspond to a moderately charged oxygen.
[b] CO charges correspond to the more common neutral adduct, slightly displaced to type II resonance structure.
[c] Fe^{III}–NO_2^- and Fe^{III}–ONO^- correspond to the complex where the N atom is bonded to the Fe (Fe-X–(Y,Y2)) and where one of the O atoms is bonded to the Fe (Fe-Y2–X–Y), respectively. For the Fe^{III}–ONO^- case, the two values at the qY correspond to qY/qY2 and dX–Y row to dXY/dXY2.

are stronger, resulting in a more robust description across different ligands. The same is true for ferric NO bound state since the NO displays NO^+ character.

It is important to emphasize that because partial charges remain fixed throughout an MD simulation, their initial assignment to a particular ligand-bound heme state will have a major impact on the accuracy of the observed active site dynamics. Table 1 reports the partial charges, bond and angle parameters for different heme–ligand coordination/oxidation states, which were carefully derived and thoroughly tested in previous works from our group.

Once the initial structure and the force field have been chosen, the system of interest can be prepared. As X-ray crystallography usually does not provide information about the positions of hydrogen atoms, they have to be added to the experimental structure. Most MD packages have an automated H-adding procedure, although some user specifications are needed. Of particular relevance in preparing globin structures are the histidine protonation states, since there are multiple tautomeric states at physiological pH. Two of tautomeric representations are neutral (with very similar *pKa* values), one protonated at the Nε (labeled HIE), and the other protonated at the Nδ (labeled HID), whereas the third state is a positively charged doubly-protonated histidine (labeled HIP). Many globins, such as Mb or Hb, have two conserved histidines: the proximal histidine F8 is a HID residue, since the Nε atom is coordinated to the heme iron and thus is deprotonated, whereas the distal histidine E7 can exist as a HIE or a HID residue. For ligand-bound cases, HIE is the more appropriate tautomeric state for the distal histidine, with the Nε–H group forming a hydrogen bond with O_2 or NO ligands. Clearly, a close inspection of the possible interactions is essential to properly describe the system.

2.3.2. Free energy calculations of ligand migration

In the study of proteins through MD simulations, relevant information about a given process is obtained from the potential of the mean force, or free energy profile (FEP) associated with the process. One of the key properties related to small ligand interactions with globins concerns the process of ligand migration from the solvent into the active site (entry process) and back (ligand escape). These processes are highly dependent on protein and solvent dynamics, the presence of specific residues acting as gates, and the tunnel cavity systems found in many globins (see Section 3.1 for particular examples) [12,61]. In order to have a quantitative description of such processes, it is necessary to study the corresponding FEP along all the paths that connect the solvent with the heme active site. There are several methods that allow the calculation of the FEP for the ligand migration process using classical MD simulations, such as umbrella sampling [62], metadynamics, [63] or Multiple Steered Molecular Dynamics (MSMD) in combination with Jarzynski's equation, which has been extensively employed by our group [12]. These three methods exhibit comparable computational costs, and offer similar statistical accuracies. The term accuracy in this case is used as a measure of the method's capacity to provide a good estimate of the reference free energy profile, which is the true profile that would be obtained with the model (i.e. the force field and system description) in the limit of infinite sampling. The main difference among these biased sampling methods relies in their practical implementations, for instance the choice of the reaction coordinate, and the type and number of simulations that need to be performed.

In an MSMD simulation, an external force pulls the system from randomly selected equilibrium configurations along a desired reaction coordinate (usually the heme ligand distance). Jarzynski's equation relates the non-equilibrium work (W), performed by the external force, to the FEP along the coordinate, $\Delta G(\xi)$:

$$\exp\frac{-\Delta G(\xi)}{k_B T} = \langle \exp[-W_i(\xi)/k_B T]\rangle \tag{2}$$

where $W(\xi)$ is the external work performed on the system as it evolves from the initial to the final state along the reaction coordinate ξ. The brackets denote the calculation of the average calculated ideally over the entire ensemble of pathways i that connect the initial with the final state. To drive the system along the desired coordinate, and to compute the work performed by the external force, a time-dependent potential is used:

$$E'(r) = E(r) + k[r-(\xi_0 + v.\delta t)]^2 \tag{3}$$

where v is the pulling speed that moves the system along the reaction coordinate, k is the harmonic external force constant, ξ_o is the starting value of the reaction coordinate and t is the MD time-step. Using this type of external potential, the irreversible work is easily computed integrating the external force, due to the potential over time, according to:

$$W(\xi) = \int_{t_v}^{t} 2k[r-(\xi_o + v.\delta t)]dt \tag{4}$$

which is usually solved numerically.

In practice, once the reaction coordinate, the pulling speed and the force constant are defined, several steered MD simulations are performed, driving the system along the reaction coordinate. For each simulation, the $W(\xi)$ profile is computed. Once sufficient $W(\xi)$ profiles are obtained (usually from 10–50), Jarzynski's equation is used to obtain the FEP or $\Delta G(\xi)$. Two parameters are critical in obtaining an accurate FEP: (1) the choice of the pulling speed and (2) the number of individual pulling simulations. For small ligand migration in globins, our experience shows that converged FEPs can be obtained using speeds of ca. 0.025 Å/ps and between 20 and 40 simulations. Usually, both entry and escape profiles are computed independently and combined to obtain a more accurate result.

A powerful alternative for sampling ligand pathways is a Monte Carlo ligand dynamics code, called PELE (Protein Energy Landscape

Exploration) [64], which has been successfully applied to several globins [44,65]. Another group of methods that allows sampling of possible small ligand migration paths in globins in a much faster, but less accurate, way are commonly used. These methods, which include the particle insertion method [16], the implicit ligand sampling (ILS) [37], and the Grid MD method [38], usually require a plain MD simulation in the absence of the ligand, and then compute the ligand migration paths. With these methods, it is assumed that the presence of the ligand has no effect on the presence of the tunnel/cavity system of the protein. With the ILS method, for example, all ligand migration paths in a globin can be readily identified using a moderate 20- to 50 ns-MD simulation [66]. The main drawback of these methods is that they tend to overestimate the presence of cavities and tunnels, and, therefore, the resulting FEPs are less accurate than those obtained by first specifying the migration pathway, for example with the MSMD method. These less expensive ligand-sampling methods should be used with care, particularly in cases where gating residues are present, since such methods may mix or even mask the presence of open and closed conformations. Ultimately, less expensive methods may be used to obtain an initial guess of the main path, which can later be analyzed in detail using more costly methods to calculate an accurate FEP. Given the variety of methods available for the study of the ligand migration process, selecting the most suitable method for a specific investigation is not trivial. In this review we will present results from our group, obtained mostly using the MSMD method, which will be analyzed in the context of experimental kinetic data. For a comprehensive and comparative review on the different methods the reader is referred to reference [12].

3. Examples Part 1. Small ligand entry and escape processes

As introduced above, ligand accessibility to the iron is controlled by several structural factors, such as the presence of internal hydrophobic tunnels connecting the solvent to the active site, the presence of specific gating residues, as well as the presence of water molecules that compete with ligands for the iron accessibility [67–69]. In this section we will report several examples of globins where the ligand entry/escape processes are characterized in detail.

3.1. Oxygen entry in Mb: the HisE7 gate pathway

The ligand migration process in myoglobin is probably one of the most-studied by both experimental and computational techniques. The HisE7 gate hypothesis was first proposed around 40 years ago, after the resolution of the first Mb X-ray structure by Max Perutz, in an attempt to explain how oxygen could reach the apparently buried heme iron [70]. The hypothesis suggests that in order to allow oxygen to reach the distal cavity, HisE7 must rotate its side-chain towards the solvent, leaving an unhindered path and thus opening the HisE7 gate (Fig. 2). The first support for this hypothesis came from experimental studies that showed that k_{on} increases when HisE7 is replaced with smaller apolar residues, such as Ala or Gly, while it decreases when replaced by larger residues as Trp [71]. Structural studies also supported the notion of HisE7 acting as a gate. Crystal structures at low pH showed HisE7 extended towards the solvent, in the so-called open conformation (as opposed to the commonly found closed conformation) [72]. Consistently, the kinetic association rate constants slightly increase when lowering the pH [73].

Another interesting feature revealed by Mb X-ray structures concerned the presence of cavities inside the protein matrix. These cavities were later characterized as hydrophobic cavities, or xenon sites, due to their capacity to hold xenon atoms. Mb, like most globins with the 3-over-3 fold, has at least 4 Xe sites, in addition to the distal pocket. These hydrophobic cavities are arranged around the heme, with Xe1 located next to the proximal HisF8 [75,76]. The presence of this tunnel cavity system in Mb suggested possible alternative

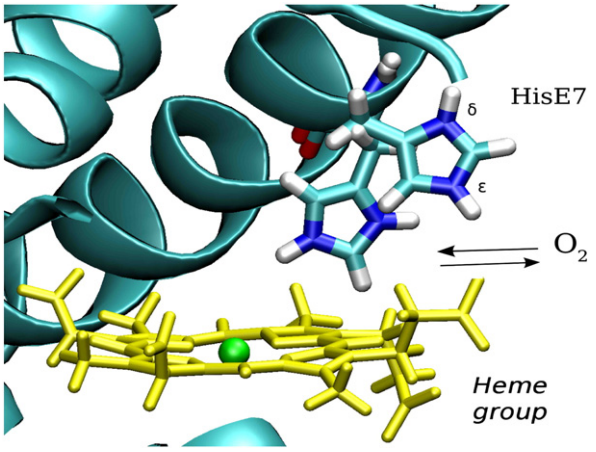

Fig. 2. Schematic representation of the HisE7 gate hypothesis, in which molecular oxygen can enter and exit the distal site due to the side-chain movement of HisE7. Both the inward (closed) and outward (open) conformations of HisE7 side chain are shown [74].

ligand entry and escape routes [20,39,40]. Regardless of this possibility, there is a general consensus that the HisE7 gate is one of the principal pathways for ligand entry in Mb [16,39,71].

Using the MSMD method, we calculated free energy profiles for oxygen migration through the E7 pathway in both open and closed HisE7 conformations. Our MD results showed that the open conformation is stabilized in both the protonated (HIP) and the neutral δ-tautomer (HID) of HisE7, due to a hydrogen bond with the backbone carbonyl of Asp 60, thus populating the open conformation even in the neutral HisE7 state. On the other hand, our results showed that neither the open nor the closed HisE7 conformations present a significant barrier for oxygen migration to the active site (Fig. 3). Instead, we identified a small free energy well along the path located at about 5 Å from the iron, which becomes deeper when HisE7 is in the so-called open state. This free energy well corresponds to a hydrophobic site that is able to accommodate an oxygen molecule, increasing thereby its effective concentration inside Mb relative to that of the bulk solvent, thus enhancing ligand uptake through the E7 pathway. Because the free energy well at this site is more pronounced in the open conformation, and the open conformation is more populated with the protonated HisE7 tautomer, this agrees

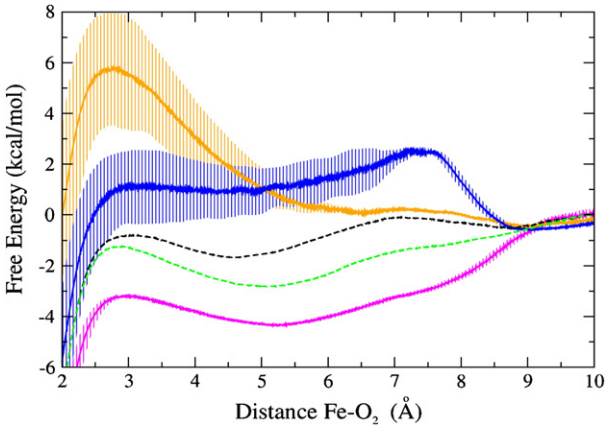

Fig. 3. Free energy profile of ligand migration through the E7 pathway for wild type myoglobin in the closed (dotted black line) and open (dotted green line) state, and mutant proteins: HisE7Ala (magenta line), HisE7Trp in the outward conformation as found in the crystal structure (blue line) and HisE7Trp in the inward conformation adopted during the simulation (orange line). The free energy was set to a value of 0 at 10 Å, where the oxygen molecule is fully solvated. Error bars represent mean square error considering the bias inherent to the Jarzynski free energy estimator for a small number of independent simulations (N = 40) (52) [74].

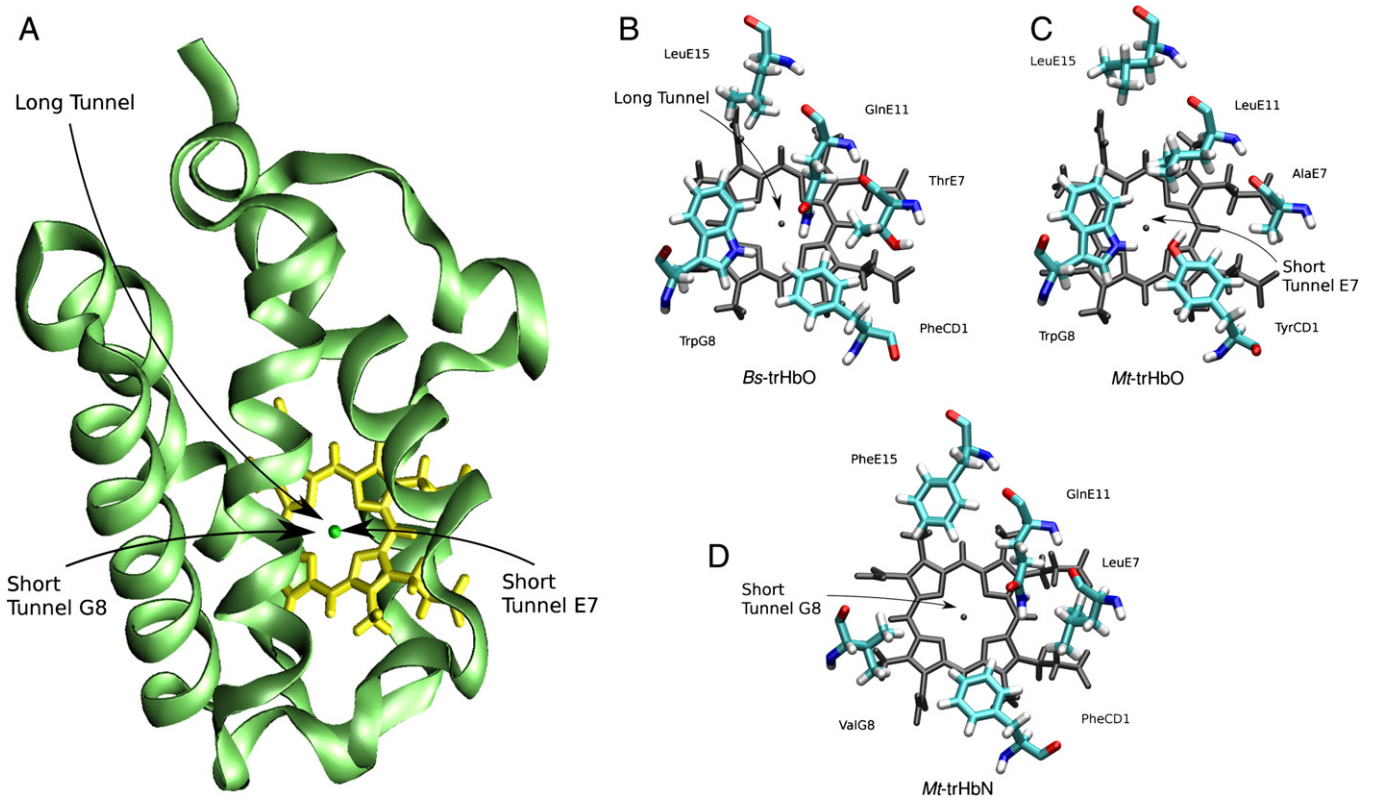

Fig. 4. A) Schematic representation of the long tunnel (LT), short tunnel E7 (STE7), and short tunnel G8 (SG8T) in the tertiary structure of *B. subtilis* trHbO (*Bs*-trHbO) [80]. Active sites of three different truncated hemoglobins are shown: Bs-trHbO (B), *M. tuberculosis* trHbO (Mt-trHbO) (C) and *M. tuberculosis* trHbN (Mt-trHbN) (D) [Milani, 2001 #539].

well with the experimentally observed increase in oxygen uptake at low pH. To further analyze the role of HisE7 in this pathway, we also computed the free energy profiles of two mutants that correspond to extreme cases of kinetic behavior: HisE7Ala and HisE7Trp, representing the fastest and slowest observed association rates, respectively [71]. The corresponding results, also presented in Fig. 3, clearly show that Trp completely fills the hydrophobic pocket and creates a high barrier for oxygen migration. In the HisE7Ala case, on the other hand, the free energy well becomes even deeper compared to the WT open conformation. The experimentally observed trend in the association rate constants, k_{on} HisE7Trp < k_{on} wt (pH 7.4) < k_{on} wt (pH 5) < k_{on} HisE7Ala, can thus be explained due to an increase in the depth of the free energy well along the E7 pathway. It is important to note that since the free energy well is created by the presence of a hydrophobic pocket, which is in direct contact with the HisE7 residue, its relative position to heme location varies slightly. Moreover, since in the MSMD simulations the oxygen ligand is explicitly considered, local side-chain rearrangements of the involved residues are observed during the migration process. A small rotation of the imidazole side chain of HisE7 and a slight displacement of the E-helix, for instance, were observed.

These results thus modify the classical concept of a "gate", imagined as a residue blocking ligand migration when it is closed and allowing passage when opened. Instead, we argue that the hydrophobic site along the E7 tunnel creates a free energy well that helps to drive oxygen uptake when HisE7 is open. This new idea reconsiders the HisE7 gate hypothesis in terms of O_2 being driven into the E7 channel by the hydrophobic effect [74]. As will be shown in the next section, oxygen escape is mainly governed by distal residues' direct interaction with the bound oxygen, and thus the observed change in the escape barrier has a negligible effect.

3.2. Small ligand access in truncated hemoglobins (trHbs) is controlled by the presence of tunnels

Despite their small size, trHbs have been found to host a tunnel cavity system that connects the active site heme with the solvent. The tunnels were first revealed in the crystallographic structure of trHbN of *Mycobacterium tuberculosis* (Mt-trHbN) [8] and later shown to be a conserved aspect of trHbs. Analysis of several trHbs structures, both in the presence and absence of Xe atoms, and kinetic studies of single point mutants allowed the identification of three potential tunnels. A long hydrophobic tunnel (LT), a short tunnel involving the G8 residue (STG8), and a short pathway involving the E7 residue (STE7) have been characterized (Fig. 4) [67,77].

Mt-trHbN is one of the most studied members of the truncated hemoglobin subfamily, and presents only two of the three potential tunnels described above, the LT and the STG8, as revealed both by both X-ray crystallography [67] and computer simulation studies [77–79]. This was one of the first proteins for which the free energy profiles for small ligand migration were determined using the MSMD method by our group, showing that both the LT and STG8 tunnels are important for the ligand entry process, and that their preferential selectivity is determined by the heme coordination state [78].

All the O and P subfamily members studied in our group, such as *M. tuberculosis* (Mt-trHbO), *Thermobifida fusca* (Tf-trHbO), *Bacillus subtilis* (Bs-trHbO) and *Campylobacter jejuni* (Cj-trHbP) have a tryptophan at the G8 position (TrpG8) which blocks the STG8 [32,81,82]. Since TrpG8 is conserved in all members of the O and P subfamilies, only the LT and STE7 are available for ligand entry in these systems. An interesting case arises in our studies of Bs-trHbO and Mt-trHbO, where the TrpG8 and E11 residues play distinct roles in the ligand migration via the LT. The corresponding FEP indicates the presence of a wide free energy well at 10 Å for both proteins, which corresponds to

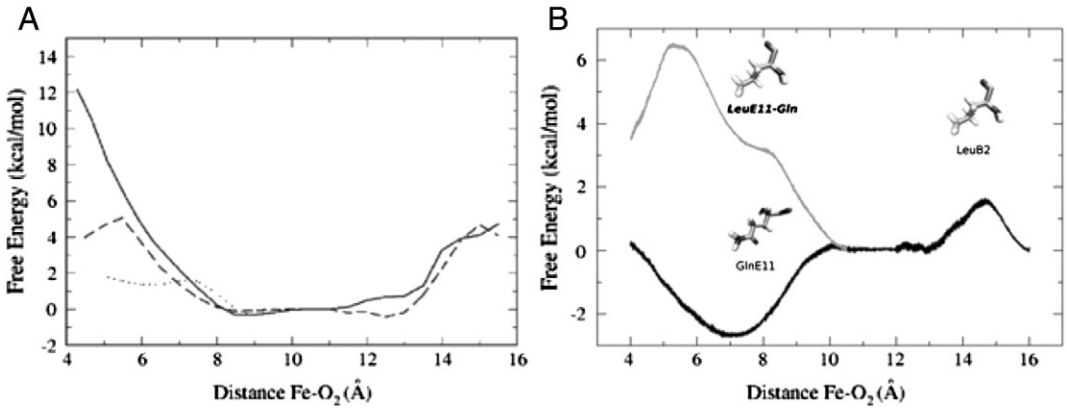

Fig. 5. Free energy profiles for ligand migration through the long tunnel. A) Mt-trHbO wild type (solid line), TrpG8-Phe (dashed line) and TrpG8-Ala (dotted line) [83]. B) Bs-trHbO wild type (black line) and GlnE11-Leu (grey line) [81].

a hydrophobic pocket (Fig. 5). From this distance to the active site, both profiles differ significantly: in Mt-trHbO a large (over 10 kcal/mol) barrier prevents the ligand from reaching the active site, whereas in Bs-trHbO no barrier is present (Fig. 5). The origin of the large barrier in the Mt-trHbO protein was traced back to the presence of the TrpG8-LeuE11 pair, which blocks the access to the heme. Consistently, mutation of TrpG8 to Phe and to Ala in Mt-trHbO resulted in a decrease of the barrier, consistent with the observed increase in the association rate from $1.1 \times 10^5\ M^{-1}\ s^{-1}$ for the WT to $1.3 \times 10^6\ M^{-1}\ s^{-1}$ for the TrpG8F mutant [82]. The interesting question is why in Bs-trHbO, where TrpG8 is present, is there no barrier for ligand migration through the LT. Detailed analysis of the MD simulations shows that GlnE11 moves towards TyrB10 in order to form a hydrogen between its amine moiety and the hydroxyl group of TyrB10, thus opening the LT for ligand entry. Since the corresponding Leu side chain in Mt-trHbO is not able to establish the mentioned hydrogen bond with TyrB10, it blocks the LT. This is observed in both the GlnE11-Leu Bs-trHbO mutant and in the WT Mt-trHbO [81].

Therefore, although Mt-trHbO and Bs-trHbO are very similar, the residue at position E11, Leu in Mt-trHbO and Gln in Bs-trHbO is able to differentially open (Bs) or block (Mt) the tunnel, allowing a faster ligand uptake in Bs, as experimentally observed (k_{on} Bs-trHbO is 100 times larger than that of Mt-trHbO) [80].

These results can be extrapolated to all the members of the O group. Sequence comparison of these proteins shows that the E11 residue is predominantly Leu or Gln, and in some cases Phe or Ser. Based on our data, a Phe residue would probably act like the Leu, closing the tunnel, whereas a Ser may act as the Gln, opening the tunnel. In this view, the O group can be divided into those with open LTs (Gln/Ser in position E11) and those in which the LT is closed (Leu/Phe). Furthermore, the correlation between the predicted open or closed LT state with the protein phylogenetic analysis highlights that this position may be a key in regulating trHb properties and, therefore, its function.

In summary, in trHbs, there are up to three possible hydrophobic tunnels that connect the bulk solvent to the heme active site. The tunnels usually display a series of free energy wells and barriers that contribute to the overall association rate. Determining which tunnel is predominantly responsible for small ligand uptake is not an easy task and requires characterization and comparison of the corresponding free energy profile. In several cases, two tunnels display similar barriers, and thus both may contribute to the entry process. The presented examples, however, clearly show how the experimental determination of kinetic association rates, for the WT and single point mutants, allows for the identification of key residues that are able to control the ligand entry and escape processes. These data, in combination with the in silico determination of the free energy profile for the same WT and mutants, elucidate molecular details of the corresponding pathway for ligand migration.

A final consideration based on the above presented results for Mb and the TrHbs can be made in relation to other ligands. For neutral ligands such as CO or NO, with net dipoles small enough to ignore, the same behavior can be expected as observed for molecular oxygen. For more polarized or even charged ligands, such as SH^-, CN^-, NO_2^- or F^-, a completely different behavior is to be expected. For such charged ligand cases, no migration free energy profiles have been reported in globins, to our knowledge, except our study of nitrate escape in Mt-trHbN. In that study, the nitrate is shown to escape directly to the solvent via none of the O_2/NO characterized migration tunnels, and the process is assisted by several water molecules that enter the protein distal site to solvate the ion [84]. This key role of water is consistent with observations performed in several studies of ion channels [85]. Thus, for highly polar or charged ligands, solvent access to the heme active site may govern the entry and escape process, and given the highly dynamic and complex behavior of solvent interactions with both ligand and protein, it is extremely difficult and computationally expensive to converge the corresponding migration profiles [66,84].

4. Examples Part 2: structure and energetics of small ligand bound globin complexes

In this section we describe the structure and energetics of small ligand-bound complexes, and in particular, how a combination of classical- and quantum mechanics-based methods is required to adequately describe these complexes. We analyze each ligand and its peculiarities separately, focusing on how the distal and proximal environments modulate the affinity. For each ligand two aspects should be considered: first, the strength of the chemical bond to the iron which depends on: i) the ligand bonding characteristics, mainly its σ-donation and π-back-bonding capacity, ii) the heme geometry, and iii) the proximal environment; secondly, the interactions between the distal environment and the ligand, once bound to the heme. Typically these are electrostatic (mainly hydrogen bond) interactions and depend on the hydrogen bond donor/acceptor capacity of the bound ligand. Each ligand will have a different behavior in each respect, and thus, globins exploiting these specific differences may become selective for a given ligand. For instance, the Fe – O_2 bond is generally weaker than the Fe – CO or Fe – NO bonds [36], and thus globins are able to mechanistically modulate their oxygen affinity, as evidenced by the range of dissociation rates, spanning 7 orders of magnitude. On the other hand, the Fe – NO bond is so strong that most globins display the same dissociation rate as observed for a free heme. In the sections to follow, globin-binding characteristics of the following ligands will be discussed in detail: O_2, CO, NO, HS^-, NO_2^- and F^-.

Table 2
Experimental k_{off} and QM/MM-calculated ΔE_{O2} for several globins and truncated hemoglobins. ΔE_{O2} values are computed using Eq. (1). Different values for ΔE_{O2} are given in cases where different conformations in the distal cavity where observed for the oxygen bound protein.

		k_{off} (s^{-1})	Distal site residues	ΔE_{O2} (kcal/mol)
Free Heme		–	–	−22.0 [9]
Mt-trHbN	Wt	0.2 [96]	TyrB10/GlnE11	−37.2 [77]
	TyrB10Ala	45 [96]		−29.8 [77]
Mt-trHbO	Wt	0.0014/0.0058 [82] 0.0025 [44]	TyrB10/TyrCD1/TrpG8	−32.92 (this work)
	TrpG8Phe	0.915 [82] 0.13 [44]		−28.6 (this work)
Mb	Wt	15 [67]	HisE7	−27.0 [30]
	HisE7Gly	1600 [98]		−22.7 [30]
Lba	Wt	5.6 [90]	HisE7	−29.7/−34.5 [89]
	HisE7Gly	3.6 [90]		−28.9 [30]
	TyrB10Ala	0.9 [90]		n.d.
	HisF8Gly + Im	15 [98]		−24.9 [30]
CerHb	Wt ThrE11Val	180 [88] 0.18 [88]	TyrB10/ThrE11	−28.6 [87] −32.0 [87]
AscHb	Wt	0.004 [67]		−34.3 [9]
PcHb	Wt	25.2 [99]	TyrB10/ThrE11	−29.1/−25.9 [89]
Cj-trHbP	Wt	0.0041 [92]	TyrB10/HisE7/TrpG8	−34.9/−31.9 [32]
	TrpG8Phe	0.033 [32]		−27.1/−38.2 [32]
	TyrB10Phe	0.0088 [92]		−30.5 [32]
	HisE7Leu	0.0003 [92]		−36.1 [32]
	TyrB10Phe/HisE7Leu	0.0028[92]		−30.4 [32]
FbHb	Wt	0.44 [100,101], 0.11(56%)/2.2(44%) [93]	TyrB10	−30.1/−20.0[97]
Pgb	Wt	0.092 [6]	No hydrogen bond	−29.6 [102]

4.1. O_2 binding

4.1.1. Distal effects

The small hydrophobic oxygen molecule adopts a negative charge density when bound to the iron, due to the significant charge transfer (π-back-bonding) from the heme group to the ligand. Thus, the coordinated O_2 interacts strongly with hydrogen bond donor residues that are properly oriented in the distal site [9] and a strong hydrogen bond network stabilizes the coordinated oxygen. This distal hydrogen bond stabilization is known as the distal effect. In many cases, the hydrogen bond network is dynamic and several conformations should be taken into account. In this context, MD simulation of the ligand-bound protein is the tool of choice in order to analyze the possible configurations that the active site can adopt. Once the relevant distal site conformations have been identified, QM/MM calculations can be performed to obtain a good description of the electronic structure of the oxy complex, and the determination of the oxygen binding energy as described in Sections 2.1 and 2.2. During the last decade, we have studied several globins using this strategy. Our results reveal that the computed binding energies show good correlation with the experimentally determined dissociation rate constants and provide an understanding of how globins regulate their oxygen affinity. Moreover, comparison of single point mutants performed in-silico also allows for the determination of individual residue contributions to oxygen affinity. Below we present several examples, highlighting their interesting peculiarities and the resulting general trends.

The first residue considered as a modulator of O_2 affinity, present in many globins, is the distal HisE7. In Mb, HisE7 establishes a moderately strong hydrogen bond with the bound O_2, and mutation of this residue to Gly produces a more than 100-fold increase in the dissociation rate constant (Table 2). Consistently, the computed oxygen binding energy ΔE_{O2} is 4.3 kcal/mol less negative when HisE7 is mutated to Gly (Table 2). Other distal residues, such as those in positions E11, CD1 and B10 in Mb and other 3-over-3 globins are usually non-hydrogen-bond-forming residues and thus do not contribute to the O_2 stabilization.

In trHbs the picture is more complex, since several distal residues in positions E7, B10, CD1 and G8 may form hydrogen bonds with the bound ligand. Among the O and P group members, TrpG8 seems to be crucial for oxygen stabilization since the k_{off} is dramatically increased upon mutation to Phe [86] (Table 2). MD simulations of several members of the O and P groups show that, in all cases, TrpG8 is tightly hydrogen bonded to the bound oxygen and significantly contributes to its binding energy [32,81,83]. All of these proteins in the O and P groups have low oxygen dissociation rates, whereas Mt-trHbN, and other members of the N group, where the hydrogen bond network is formed by TyrB10 and GlnE11, do not have Trp at G8 position and have high oxygen dissociation rates, [68,77]. Our calculations show that both residues interact with the bound oxygen, but TyrB10, a residue present also in many other TrHbs is the main contributor to oxygen affinity.

4.1.2. Dynamic aspects of the distal effect

In some cases, the observed O_2 affinity does not agree with the affinity anticipated by examining solely the distal site amino acid composition. In these cases single point mutations may lead to confusing results. The origin of these discrepancies is often related to dynamic effects that allow the distal site to adopt significantly different conformations. In such cases, the observed k_{off} is the result of a combination of the individual rates (or affinities) for each conformation, weighted by their differential populations in the configurational space.

In this section we present several examples where multiple conformations in the distal cavity were found to differentially modulate O_2 affinity: the *Cerebratulus lacteus* mini-hemoglobin (CerHb), the *Paramecium Caudatum* truncated hemoglobin (Pb-trHb), *C. jejuni* truncated hemoglobin P (Cj-trHbP), soybean leghemoglobin (Lba), and *Escherichia coli* flavohemoglobin (FbHb). The results for each case are briefly described below and summarized in Table 2.

CerHb mini-hemoglobin displays a distal pocket with three hydrogen bond donor residues TyrB10, GlnE7 and ThrE11. Although the protein shows the typical TyrB10 and GlnE7 pair, unlike *M. tuberculosis*, its k_{off} is quite high (Table 2). Moreover, mutation of TyrB10 to Phe has little effect on the dissociation rate, and intriguingly, mutation of ThrE11 to Val reduces the k_{off} by three orders of magnitude. Using a combined MD and QM/MM strategy, we were able to solve this apparent discrepancy [87]. Results from the MD simulations indicate the presence of two different conformations, separated by a small (1–2 kcal/mol) free energy barrier (Fig. 6). In the first conformation, in which oxygen binds tightly, the TyrB10 residue forms a hydrogen bond with the bound O_2. This conformation (Cf1) is a high-affinity conformation, with a calculated ΔE_{O2} of −33 kcal/mol. In the second conformation, the TyrB10 hydroxyl group rotates to interact with the ThrE11 hydroxyl group, resulting in a low-affinity confirmation ($\Delta E_{O2} = -24$ kcal/mol). The observed dissociation rate can be explained only by considering the

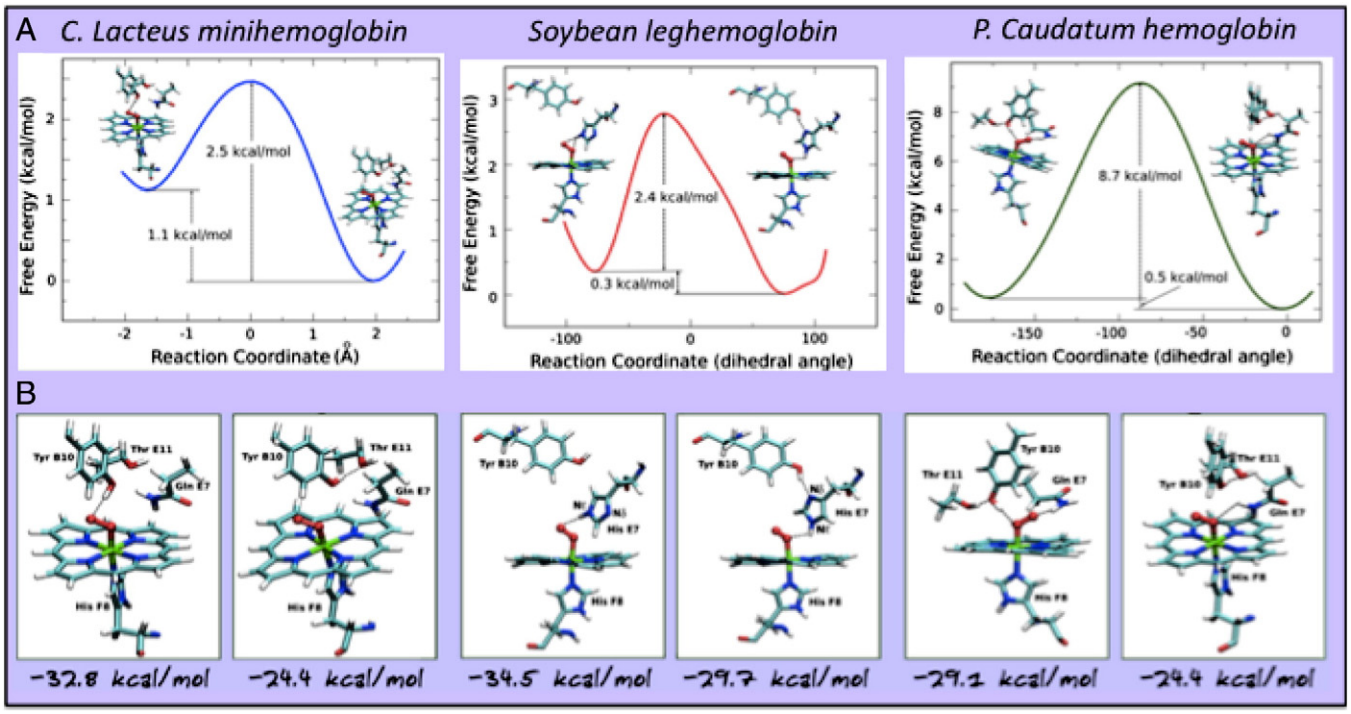

Fig. 6. Three examples of globins that display two distal cavity conformations, which possess high and low O_2 affinity. A) Free energy profiles for the conformational interchange processes in CerHb, PcHb and Lba. B) QM/MM-optimized structures of the two conformations found in each distal site. High and low affinity conformations are shown in left and right panels, respectively. The QM/MM-calculated ΔE_{O2} is shown for each conformation.

dynamic equilibrium between both conformations. Moreover, the results clearly explain how the mutation of ThrE11 to Val, which eliminates the low affinity conformation, results in the dramatic 1000-fold reduction of the k_{off}, since only the high affinity conformation is retained. Indeed, the calculated ΔE_{O2} for the ThrE11Val mutant was −32 kcal/mol. This result, together with the lack of the low-affinity conformation, confirms the proposed equilibrium in the distal cavity (Fig. 6) [88]. Pc-trHb, also containing TyrB10, GlnE7 and ThrE11 in the distal cavity, is very similar to CerHb. In fact, the results from MD and QM/MM simulations indicate a very similar mechanism, as described for CerHb, which accounts for the unusually high k_{off} (Table 2 and Fig. 6) [89].

Among the 3-over-3 globins, Lba is a well-known case in which distal stabilization does not follow the expected trend on the basis of the distal cavity amino acid composition. As in Mb, HisE7 is present in the Lba distal cavity. In contrast to what is observed in Mb though, site-directed mutagenesis studies showed that, in Lba, HisE7 does not significantly contribute to O_2 stabilization [90]. Indeed, changing HisE7 to non-hydrogen-bonding residues has an almost negligible effect. Surprisingly, the oxygen affinity of Lba is even larger than that of Mb (Table 2) [91]. In order to explain this apparent discrepancy, it was proposed that an alternative HisE7 conformation exists, in which a hydrogen bond between HisE7 and TyrB10 lessens the interaction between HisE7 and O_2 [90]. The existence of this alternative conformation, with low O_2 affinity, was confirmed by MD simulations and QM/MM calculations [89]. In the high-affinity conformation, HisE7 forms a strong hydrogen bond with bound O_2. In the low-affinity conformation, though, the HisE7 imidazole group rotates through its Cβ–Cγ angle, and forms a hydrogen bond with TyrB10, weakening the interaction with O_2. ΔE_{O2} calculations confirm the difference in affinity between the two conformations. MD simulations and calculated FEPs provide insight into their relative populations. In this case, both conformations are separated by a low free energy barrier of interconversion (2.4 kcal/mol), and are equally populated in the conformational ensemble. Although the presence of a low-affinity conformation in Lba could be responsible for reducing the effect of the HisE7 substitution, the presence of a hydrogen-bonded conformation still seems to be inconsistent with the experimentally observed trend. As will be discussed in Section 4.1.3, the complete understanding of this intriguing mutant requires consideration of the proximal environment.

Another complex example of multiple conformations can be found in the case of the truncated globin Cj-trHbP [92]. Experimental data reveals a very low dissociation rate for the wild type Cj-trHbP ($k_{off} = 4.1 \times 10^{-3}\ s^{-1}$). Interestingly, the dissociation rates for all the mutants TrpG8-Phe, TyrB10-Phe, HisE7-Leu and TyrB10-Phe/HisE7-Leu did not result in significant differences. Recently, we have shown the existence of a redundant distal site cavity with an extremely atypical behavior, which seems to be present in the Group III member Cj-trHbP (Table 2) [32].

Finally, the last example is represented by the *E. coli* flavohemoglobin (FbHb) [93,94]. FbHb possesses nitric oxide dioxygenase activity [93,95], as in the case of Mt-trHbN [77,78,96]. FbHb has a very high oxygen affinity (Table 2). In a recent work we have shown that the high oxygen affinity can be explained by the presence of a water molecule in the active site, which forms a hydrogen bond with O_2 and acts as a bridge between O_2 and TyrB10 [97]. The resulting conformation presents a high oxygen affinity, even higher than the conformation with TyrB10 directly forming a hydrogen bond with O_2 [97].

Taken together, the different examples presented here highlight the importance of the dynamic nature of the distal cavity. For this reason, computer simulations can provide very valuable information in order to determine the molecular basis of oxygen affinity regulatory mechanisms, complementing and expanding the information obtained by crystallographic, mutagenesis and spectroscopic data. In many cases, the simulations also reconcile experimental results that appear inconsistent at a first glance.

4.1.3. Proximal and heme conformational effects on oxygen affinity

Despite accounting for both the static and dynamic distal effects, several cases are reported for which this information does not

sufficiently explain the modulation of oxygen affinity [30,102]. In many of these cases, intrinsic effects associated with the heme group have been implicated. Among these effects, we can distinguish proximal effects (associated with the position and environment of the proximal histidine, HisF8) [30] from distortions of the heme group (also modulated by the heme environment) [102]. In the following sections we describe the molecular basis of these two types of regulatory mechanisms.

4.1.3.1. Proximal effects. Since the proximal histidine is able to modulate ligand affinity (trans-ligand effect) we have studied the regulation of O_2 affinity by means of proximal effects. A classical example of proximal effects has been observed in Lba, as introduced in Section 4.1.2. Since it was shown that HisE7 does not stabilize O_2 in the binding site, it is difficult to explain the larger O_2 affinity compared to Mb. In this context, we [30] and others [98] have shown that proximal effects also play an important role in regulating O_2 affinity in Lba. The specific proximal effects we have studied involve (i) the charge relay from the HisF8 to the heme iron, (ii) the rotational position of the HisF8 imidazole ring, and (iii) the distance between the HisF8–Ne and the heme iron (Fig. 7).

(i) The charge relay mechanism is determined by the charge transfer capacity of the HisF8 to the iron, which stabilizes the iron–oxygen bond through π-backdonation from the iron [103–105]. The modulation of the charge transfer capacity occurs through the hydrogen bond interactions that the HisF8–NHδ forms with the protein environment, which in turn, modulates the basicity of the imidazole ring, and consequently its charge. We have observed that neither a very weak hydrogen bond interaction (as in the case of a H_2O molecule) nor a very strong one (as the one formed with a carboxylate group) corresponds to the maximum oxygen affinity. Indeed, an intermediate hydrogen bond strength, for example with a carbonyl group, results in a maximum O_2 affinity (being 6.5 kcal/mol higher than the case of the carboxylate hydrogen bond, and 2.7 kcal/mol higher than the weak water hydrogen bond) [30].

(ii) The rotational position of the histidine is defined as the position of the plane containing the proximal histidine imidazole group of the proximal histidine relative to the line that joins two opposite pyrrolic nitrogen atoms (Fig. 7). If the plane is aligned with this line, the conformation is called "eclipsed", but if it forms an angle of 45°, it is called "staggered", which results in a slightly more favorable oxygen affinity. Crystal structures of Mb [7] and Lba [106] and QM/MM calculations [30], show that while in Mb the imidazole ring is in the eclipsed conformation, it is closer to the staggered conformation in Lba, also contributing to its overall higher oxygen affinity. Indeed, the staggered conformation enhances O_2 affinity by 1 kcal/mol, but this is increased to 3 kcal/mol in the presence of a carbonyl group forming a H-bond with the proximal imidazole [30].

(iii) The third effect is determined by the distance between the heme–iron and the coordinated proximal HisF8–Nε. The relative position of the proximal histidine with respect to the heme group is determined by the hydrogen bond interactions between HisF8 and the other proximal residues. Through these interactions, the protein is able to constrain the position of the histidine, relative to the heme group, and, therefore, modulate oxygen affinity. We have observed that constraining the Fe–His distance to shorter than the equilibrium distance in the isolated active site can increase O_2 affinity by ~1.5 kcal/mol. Similarly, O_2 affinity is decreased when the proximal histidine is pulled away from the heme. Once again, QM/MM calculations show that while Lba displays an Fe–His distance of 2.04 Å, in Mb this distance is 2.18 Å, being the equilibrium distance in solution 2.12 Å. In this context, it is clear that Lba regulates O_2 affinity by orienting the proximal HisF8 closer to the heme–iron. Thus, the absence of the anticipated dramatic

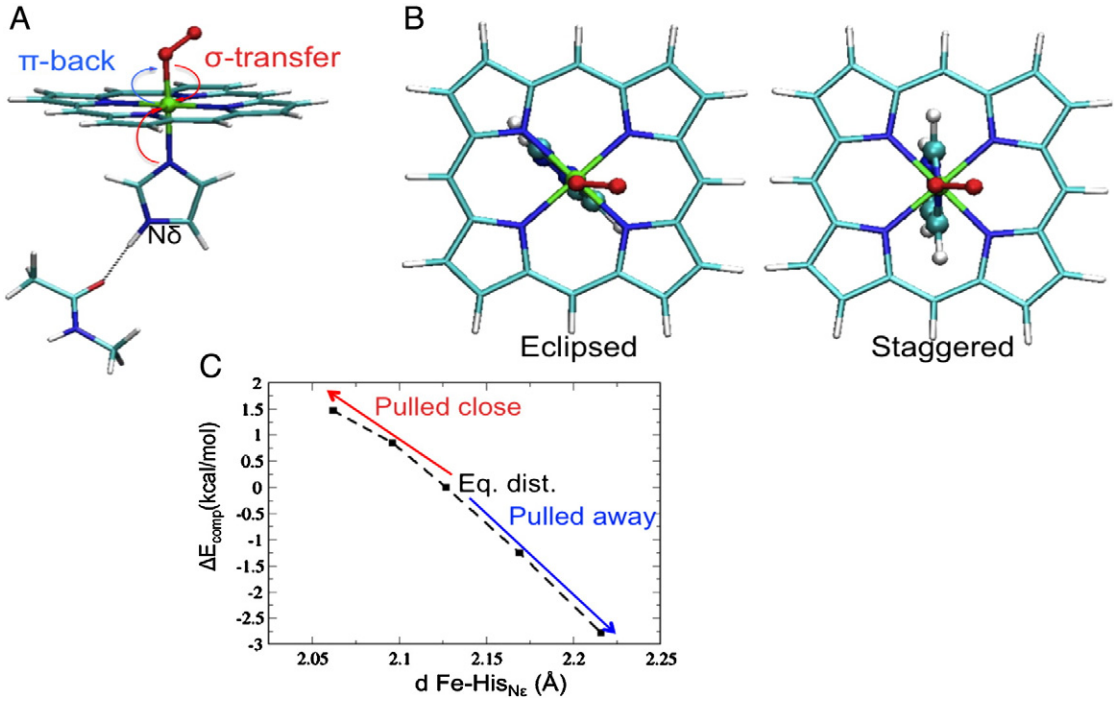

Fig. 7. The three types of proximal effects observed in globins. A) Charge relay from the HisF8 to the Fe, enhanced by hydrogen bond interactions with the surrounding residues. B) Rotational position of the HisF8. C) Effect of the Fe–His distance: ΔE_{comp} corresponds to the difference between the ΔE_{O2} at a given Fe–HisF8 distance and the ΔE_{O2} at the equilibrium (unrestrained) Fe–HisF8 distance.

increase in k_{off} due to the HisE7Gly mutation in Lba (described in Section 4.1.2) can be better explained by its high oxygen affinity modulated by all the three types of proximal effects, rather than solely considering the equilibrium of low- and high-affinity distal site conformations [30].

The present analysis of the proximal effects in globins has great significance when analyzing the cooperative regulation of oxygen affinity in mammalian hemoglobins. Although the mechanism by which this regulation is achieved is still under large debate [107], the proximal effects can have a prominent role in this regulation. For instance, it is known that for the R-subunits in the T-state, the proximal His is pulled away from the iron, and relaxes when transitioning to the R-state [108]. In this context, the pulling effect of the proximal histidine could be one of the causes of the difference in oxygen affinity between the T and R states.

4.1.3.2. Modulation by heme structure. The last mechanism that allows for a subtle regulation of oxygen (and other ligands) affinity in heme proteins is the heme structure itself. For example, chemical modification of the substituents (or side chains) of the porphyrin ring determines the fine tuning of the iron reactivity, as has been shown using synthetic porphyrins. This mechanism, however, is not widespread in naturally occurring heme groups, and is limited to only some particular organisms [109]. The electronic properties of the porphyrin ring reside in the nature of its structure. In the absence of constraints, a porphyrin will adopt a planar D_{4h} symmetry. Interactions with the protein environment, however, produce distortions in this planar structure, which in turn modify the electronic structure and ultimately the affinity for oxygen and other small ligands [110]. To study the consequences of heme structure on its reactivity, a systematic classification of heme distortions, referred to as normal coordinate structural decomposition (NSD), has been proposed by Janzen et al. [111]. In their proposal, the authors identified the most important out-of-plane (saddling, ruffling, doming, X-waving, Y-waving, and propellering) and in-plane (meso-stretching, N-pyrrole stretching, pyrrole traslation (X, Y), breathing, and pyrrole rotation) normal modes that relate the structure of a distorted heme compared to an ideal reference D_{4h} structure [112,113] thus allowing a systematic analysis of the heme structure. It should be noted that similar heme distortions are common within subfamilies, suggesting that the observed distortion could be functionally relevant [111,114]. Besides their potential role in functional-family classification, the effect of heme distortions in particular protein cases have been studied in relation to their UV–vis, resonance Raman spectra, redox potential, and ligand affinity [110,112,115–121].

A recently reported extreme case of heme distortion is presented by the *Methanosarcina acetivorans* protoglobin (Pgb), a single domain archeal globin that tightly binds O_2 due to its low O_2 dissociation rate (0.092–0.0094 s^{-1}). Strikingly, the Pgb structure shows no distal hydrogen bond stabilization of the heme-bound O_2, thus raising the question as to how the low dissociation rate is achieved [6]. In order to analyze the effect of heme distortions on O_2 affinity, we used the QM and QM/MM types of calculations to determine the oxygen binding energy as a function of each possible normal mode related to the heme distortion [102]. In this way, we computed the energy required to distort the heme along each mode in the absence (red line) and in the presence of the oxygen (blue line) as shown in Fig. 8 top panel, for the ruffling and breathing modes. It can be seen that for all modes, distortion of the heme increases the energy. However, the increase is different for the free and bound states, and, thus, the difference between both curves, representing the change in the ligand binding energy with respect to the ideal planar heme, may increase for both positive and negative distortions (as for ruffling) or even decrease (i.e. become larger and thus represent a higher affinity) as for positive breathing motions.

Besides the two examples shown in Fig. 8, the overall results show that almost all the out-of-plane and in-plane distortions lower the affinity for O_2. The only mode that has the ability to strongly modify the affinity, either increasing or decreasing it, is the compression–expansion mode called breathing shown above. The origin of this behavior is that for most modes, especially those involving out-of-plane movements, the unbound heme is softer than the ligand-bound heme. In the breathing mode, which represents an in-plane distortion, compression possibly increases the electron density of the iron and the π-back-donation, similar to the proximal effect mentioned previously, and thus increases affinity.

Analyzing the NSD of the Pgb crystal structure, we found a very strong compression of the ring besides the clear out-of-plane

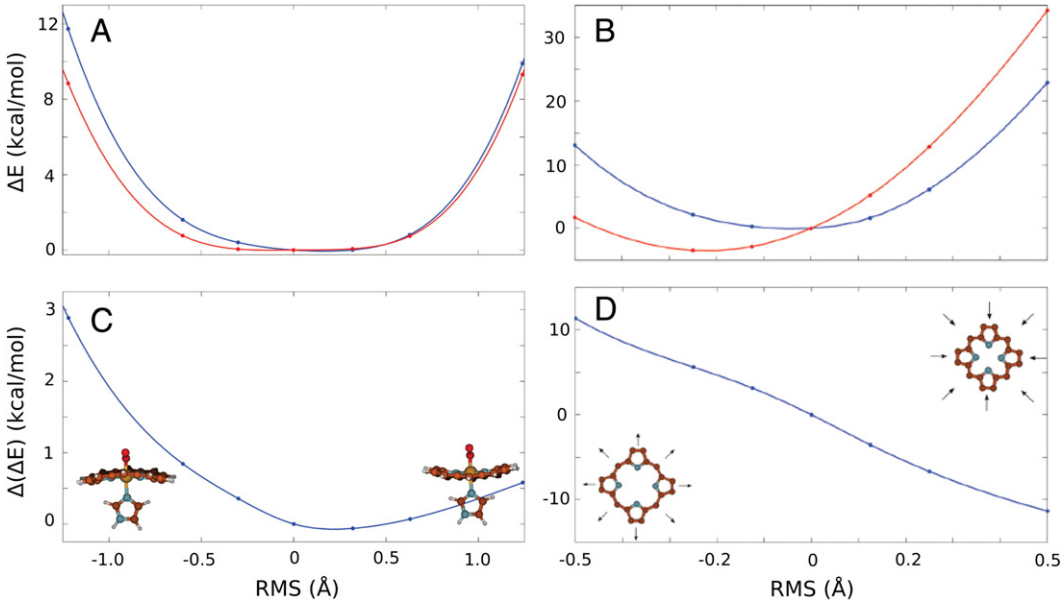

Fig. 8. Comparison between ruffling (A and C) and breathing modes (B and D). Top panels present the cost profiles (kcal/mol) for the heme distortion of the oxy (blue) and deoxy (red) structures. The difference between these two curves is depicted in the lower panels. The reference energy difference corresponds to the non-distorted heme. The x-axis represents the distortion (Å) from the reference structure.

distortion already mentioned. This distortion could explain the high affinity for O_2, taking into account the absence of distal residues that can exert hydrogen bonding stabilization. In fact, according to the quantum calculations, the distortion observed in Pgb corresponds to ca. 2–4 kcal/mol O_2 affinity enhancement with respect to a planar structure. QM/MM calculations confirmed a gain of 7.6 kcal/mol for the binding energy with respect to the isolated heme. This value is comparable to that expected for an enhancement of the affinity due to 1–2 distal hydrogen bonds. These results reinforce the importance of the distortion of the heme in order to understand how the properties of a particular heme-protein can be regulated and finely tuned [102].

4.2. CO binding

CO complexes differ from O_2 and others complexes in the following ways: i) in absence of any constraint, Fe–C–O presents a linear configuration, contrasting with the bent structures observed for instance in O_2 or NO complexes, and ii) CO is a very good π acceptor, which allows the existence of two resonance structures, which depend on the electronic density of the distal cavity. In particular, polar interactions and the formation of hydrogen bonds between the bound CO and the distal residues increase the extent of back-donation from the Fe d to the CO π^* orbitals. As a consequence, the Fe – C bond strengthens while the CO bond weakens. In this context, CO is a useful vibrational probe of heme binding sites in proteins, because Fe – CO back-bonding is modulated by polar interactions with amino acid residues, and by variations in the donor strength of the trans ligand. This modulation can be monitored sensitively by the C – O and Fe – C stretching frequencies, which are readily detectable in infrared (IR) and resonance Raman spectra. Therefore, CO is very often used as a probe for investigating distal environmental effects on ligand binding of heme. For example, in Bs- and Tf-trHbO, resonance Raman and IR measurements identified two CO conformers determined by specific interactions with the distal residues, with a moderate or a strong positive environment around the CO-bound Fe [122,123]. For Bs-trHbO, classical MD simulations show that the coordinated CO interacts strongly with TrpG8 and weakly with GlnE11, which pivots forming and breaking the bond with the coordinated CO [81]. For Tf-HbO the spectroscopic and computational results demonstrate that CO interacts with TrpG8 and also with both TrpG8 and TyrCD1 in a dynamic interplay. TyrB10 does not interact with the bound CO [123].

A particularly interesting case is that of the CerHb which contains TyrB10, ThrE11 and GlnE7 in the distal cavity, as in many other globins. Whereas in many trHbs, mutagenesis of the distal residues, typically in the E7 and B10 positions, shows an increased ligand dissociation rate, replacement of ThrE11 to Ala in CerHb leads to a surprising reduction of the k_{off} [88]. MD simulations of the CerHb-CO derivative revealed two conformations with different stabilizing hydrogen bond networks, similar to that obtained for the oxygenated species [87]. While in the conformer 1 the ligand is stabilized by a hydrogen bond with TyrB10 like in many other truncated globins, in the conformer 2 TyrB10 instead establishes a hydrogen bond with ThrE11 instead of with the CO ligand. In this second conformation, the position of the ThrE11 is fixed by a hydrogen bond with GlnE7. QM/MM calculations over both conformations reveal a modest decrease in ligand stabilization (−48.5 kcal/mol to −45.6 kcal/mol, respectively), undoubtedly due to the minor sensitivity of the CO ligand than the O_2 ligand to the environmental changes (see above). Binding energies and geometrical parameters were compared with the corresponding isolated Fe(II) hexacoordinated porphyrin complex, with imidazole and CO as the axial ligands. The new conformer 2, observed in the MD simulations of the WT CerHb, is characterized by very similar binding energy and geometrical pattern as found for the ThrE11-Val mutant and the isolated complex. Consequently, a static visual inspection of the X-ray structure inadequately explains the experimentally characterized behavior of CerHb with small ligands, and does not support the seven-fold decrease in the experimental ligand dissociation rate constant for the mutant CerHb.

Similarly, resonance Raman (RR) experiments of CO bound flavohemoglobin (FHb) suggested the presence of two different conformations, which were assigned as open and closed conformations of the distal pocket [124]. The RR frequencies of the closed conformation are compatible with the presence of a strong hydrogen bond between the ligand and a distal residue, while in the open conformation no strong hydrogen bond is present. Moreover, both conformations appear to be in dynamic and pH-dependent equilibrium: an increase in pH increases the relative population of the open state [124]. Classical MD simulations show that a conformation with a bridging water molecule hydrogen bonded to the bound CO is present for a significant portion of the simulation time, alternating with another conformation where the hydrogen bond is absent [97]. The analysis for the CO-bound protein showed that the hydrogen bond is formed 20% of the simulation time, strongly suggesting that the closed conformation corresponds to the bridging water, while the open conformation should correspond to those where no water molecule or hydrogen bond is present. To further validate the pH dependence, MD simulations of the CO complex with a charged TyrB10 were performed, revealing that, once TyrB10 is deprotonated, it swings out from the active site and, therefore, water can no longer be tightly hydrogen bonded to the bound ligand.

4.3. Fluoride binding

Fluoride is a common ligand for heme proteins in the Fe(III) state. It is not known as a physiological ligand, and only recently has it been reported that it can modulate the reactivity of a heme protein [125]. However, the spectroscopic properties of the fluoride complexes provide a simple and direct method to monitor the interactions of the distal heme pocket environment with the iron-bound ligand [126].

As hydrogen bonding is the only effective stabilization mechanism for the heme-bound fluoride, the high sensitivity of fluoride complexes can be used to probe hydrogen bonding in the distal cavity of heme proteins. A very good correlation between the vibrational and electronic features has been found for various fluoride complexes of heme containing peroxidases providing a simple method for testing the polarity of the distal cavity [127]. Recently, the combination of UV–vis and RR with MD simulations has been applied to study the fluoride complexes of native and mutant forms of Tf-HbO.

We have exploited the TyrCD1, TyrB10 and TrpG8 single, double and triple mutations to Phe, to perform a detailed study of the hydrogen bond interactions between the protein and heme-bound fluoride. All the techniques yield evidence that TrpG8 and TyrCD1 can form strong hydrogen bonds with fluoride, whereas TyrB10 plays only a minor role in the stabilization of the ligand. The same result has been observed for both the O_2 [32] and CO adducts [123]. However, when the effects of the mutations on the RR spectra are compared, it can be seen that the data obtained from CO complexes and those obtained from fluoride complexes can be explained assuming similar hydrogen bonding patterns. The corresponding complexes exhibit different behaviors, however, since back-bonding in the CO complexes depends on all kinds of polar interactions with the neighboring amino acids, while hydrogen bonding is the only effective stabilization mechanism for the heme-bound fluoride. Moreover, the two types of complexes have different chemical properties, namely (i) carbon monoxide is neutral (and almost apolar), whereas fluoride retains a negative charge, and (ii) hydrogen bonding to CO is directional, whereas there is no directionality in F – HX bonding because of the monoatomic nature of the fluoride ligand.

4.4. NO binding

Nitric oxide (NO) is a very important heme ligand, since it is related to the modulation of several fundamental biological processes, like vasodilation and inhibition of platelet aggregation [128,129]. In mammals, NO binds to the heme-containing enzyme soluble guanilate cyclase (sGC). NO binding to sGC results in the cleavage of the proximal Fe–His bond, as a result of the negative trans effect. It is assumed that the breaking of the proximal Fe–His bond gives rise to a conformational change which in turn activates the enzyme [130,131]. DFT calculations performed by our group on model systems have shown that the negative trans effect and the breaking of the Fe–His bond are related to the hydrogen bonding network of the proximal histidine [132], which affects (as explained in Section 4.1.3) the charge density on the proximal histidine. Model system calculations indicate that in the extreme case of a completely deprotonated imidazole, the Fe–His bond is reinforced enough to avoid the trans effect. Intermediate cases (represented by the active sites of Hbα and β, the O_2-sensing protein FixL and the horseradish peroxidase C) were also considered. The observed trend suggests that the stronger the hydrogen bond of the proximal histidine, the higher the Fe–His dissociation energy, and the lower negative trans effect. The results correlate well with the Raman υ(Fe–His) stretching frequencies measured for these heme proteins. An interesting example of this effect is cytochrome c′ (Cyt c′), a protein that has several similarities with sGC. This protein has a very high υ(Fe–His) frequency (231 cm^{-1}) [133], however, the cleavage of the Fe–His bond after NO binding has been observed [133]. QM/MM calculations showed that this apparent inconsistency may owe to the existence of an alternative conformation for the proximal histidine when dissociated from the heme [134]. In this context, it is clear that not only the nature of the Fe–NO bond is responsible for the trans effect, but also the ability of the protein matrix to accommodate the proximal histidine in the unbound state.

4.5. Nitrite binding

The reduction of nitrite (NO_2^-, pKa 3.15 at 298 K) [135] to nitric oxide (NO) (Fig. 10A) by denitrifying metalloenzymes is an important component of the global nitrogen cycle. Heme-containing nitrite reductase (NiR) enzymes perform such nitrite reduction, which is proposed to occur after direct binding of the nitrite anion to the heme iron center. It is well known that this reaction is performed by denitrifying bacteria and it has been extensively studied for these organisms [136–140]. In the last 10 years, however, substantial evidence started to appear showing that metalloenzymes, like Hb and Mb, present in mammalian tissues, can also reduce nitrite to NO under physiological hypoxic conditions [141–147]. The relevance of such a finding is that this pathway may circumvent the O_2-dependent NO synthase pathway.

Based on calculations and structural findings, it has been proposed that nitrite reduction can, in principle, occur by either the energetically feasible N-bonded "nitro" or O-bonded "nitrito" modes (Fig. 9B). For the nitro mode it is widely accepted that a formal double protonation of the O-atom precedes the release of a water molecule and generation of a Fe^{III}-bound NO which then dissociates from the ferric heme [137–139,148,149]. In contrast, protonation of an O-bounded nitrito ligand would generate the ferric-hydroxo species and NO through an ON–O bond homolysis reaction (Fig. 10B) [60,150]. Moreover, recently it has been shown that the NO produced by the deoxy-Hb reduction of nitrite may react with the nitrite-bound met Hb^{III} to yield the N_2O_3 species [151,152], which may play a key role in nitrite-dependent signaling. This finding implies that hemoglobin may act as an allosterically regulated enzyme that converts two nitrite ions into an N_2O_3 molecule (Eqs. (5) and (6)).

$$\text{Heme–Fe(II)} + NO_2^- + 2H^+ \rightarrow \text{Heme–Fe(III)} + NO + H_2O \quad (5)$$

$$\text{Heme–Fe(III)} + NO_2^- + NO \rightarrow \text{Heme–Fe(II)} + N_2O_3 \quad (6)$$

Whether the nitrite reduction occurs in a catalytic fashion Eqs. (5) and (6) or not Eq. (5), both mechanisms imply coordination of nitrite anion to Fe^{II} and/or Fe^{III} species. Among the several coordination modes of nitrite anion to metals, the predominant and thermodynamically favored mode to Fe(II) and Fe(III) is the N-mode "nitro" [153–156]. Computational results, however, suggest that linkage isomerism may not be unlikely, and the availability of proton donors in the distal pocket may affect the balance between the O-bound and N-bound isomers (see Fig. 10) [60,150,151].

The crystal structures of the nitrite adducts of cytochrome *cd1* NiR from *Paracoccus pantotrophus* [136], cytochrome *c* from *Wolinella succinogenes* [157] and sulfite reductase (SiR) heme protein from *E. coli* [158], clearly reveal the N-nitro binding mode. These proteins have more than one distal pocket hydrogen bond

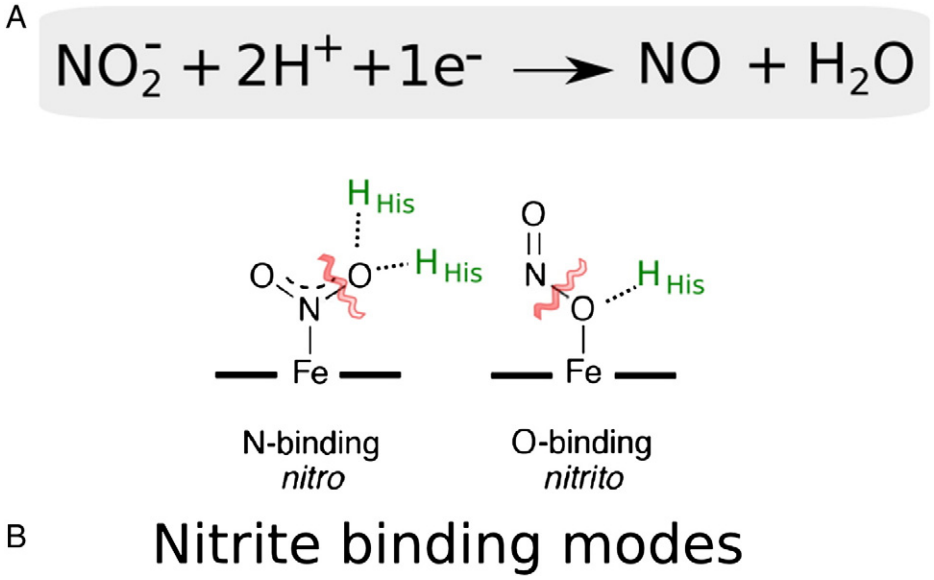

Fig. 9. A) Dissimilatory reduction of nitrite to NO performed by heme proteins. B) Different nitrite binding modes found for mammalian hhMb and human deoxy-Hb.

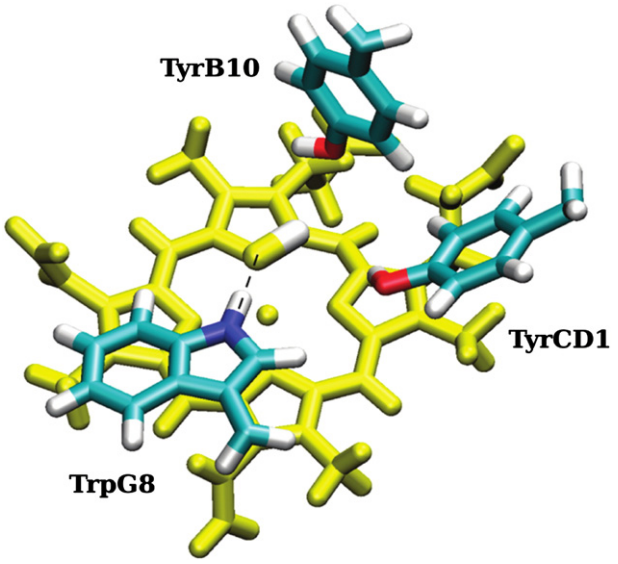

Fig. 10. Schematic representation of the WT Tf-trHb distal site with coordinated HS^-, showing the residues of the distal site (TrpG8, TyrCD1, and TyrB10). [59].

interaction with the bound nitrite, which is not the case for mammalian horse heart myoglobin (hhMb) and human hemoglobin (Hb) where only one distal pocket hydrogen bond interaction could be made. It has been recently shown that nitrite binds to the ferric centers of $hhMb^{III}$ and human Hb^{III} not through the common "nitro" mode, but rather through the unusual (for heme proteins) O-binding "nitrito" mode [159,160]. After several unsuccessful attempts to obtain the physiologically relevant nitrite coordinated to Fe^{II} species, it was finally generated by photoreduction of the Fe^{III} species. Although it may not represent the true equilibrium structure of the reactive Mb^{II}-nitrite compound in physiological conditions, the fact that the nitrito mode is retained for the Fe^{II} species reinforces the proposition that this may be a relevant binding mode for these mammalian heme proteins [161].

A key question is, what controls the binding mode of nitrite to mammalian hhMb or Hb and how that is related to the NiR activity of these heme-proteins. It has been hypothesized that the single hydrogen bonding HisE7 directs the nitrite towards this O-binding mode and influences the subsequent nitrite reduction kinetics. This hypothesis was tested and confirmed through the study of two different mutants for hhMb; HisE7-Val and the double mutant HisE7-Val/ValE10-Arg [160]. These two mutants showed for the first time the nitrite coordinated in these different modes in the same heme protein.

QM studies have reported that for an Fe(II)-porphyrin model system; the N-bonded nitro form tends to be favored over the O-bonded nitrito form by ~7 kcal/mol [146]. We have performed QM/MM simulations for individual α and β Hb^{II} subunits and showed that the N-bound isomer of nitrite is favored over the O-bound form by 9 kcal/mol for the α but only 3 kcal for the β [60]. MD simulations studies were also done in that work for human Hb^{II} (T state) showing structural features of the N-bound and O-bound nitrite hydrogen bonding interactions with the distal histidine that could contribute to the NiR activity [60]. These findings suggest that both binding modes in the ferrous system could contribute to NiR activity, in particular the O-binding mode has the advantage of requiring a single proton transfer (Fig. 9) that will lead to the formation of NO, and could take place before linkage isomerism to the thermodynamically favored N-mode.

Taken together, the computational results and structural findings suggest that the linkage isomerism is feasible and that hydrogen bonding a distal pocket residue can direct the bound nitrite anion toward the O-nitrito mode and can affect the NiR activity. The calculated energy differences between the N- and O-binding modes of nitrites to hemes are on the order of hydrogen bond stabilization energies, and in accordance to this, structural findings showed that nitrite binding mode depends on the presence of hydrogen bonding residues in the distal pocket environment.

In a general context, the single distal residue HisE7 in hhMb or in Hb, is a crucial factor in the nitrite reduction by Mb and Hb. In accordance to that, the rate constant for the same reaction catalyzed by bacterial heme proteins (two distal histidines) is much larger than that of the deoxy Mb and Hb, suggesting that this difference is, among other factors, related to the availability of hydrogen bond donors in the distal site. Interestingly, substitution of either of the two invariant histidines with alanine has a dramatic effect on nitrite reduction by *Pseudomonas Aeruginosa* and the activity resulted to be ~1% of the WT [149].

These key differences in the active sites between bacteria and mammalian heme proteins have been recently studied using molecular modeling combined with dynamics simulation for rationally designed artificial NiRs based on Mb mimicking cytochrome cd1 NiR [162].

4.6. Sulfide binding

The first high-affinity sulfide binding hemoglobin studied was the hemoglobin I (HbI) from the mollusk *Lucina pectinata*, that binds sulfide in its ferric state and works as a sulfide carrier [163]. Two members of the trHb family, Bs-trHbO and Tf-trHbO, were recently found to have high affinity for sulfide species [59]. Both proteins have a dissociation rate constant much lower than that reported for myoglobin, but still 10 times larger than *L. pectinata* HbI hemoglobin [163]. Given the potential sulfide binding properties of hemoglobins and the active sulfur metabolism of microorganisms, biochemical functions other than transport of the gaseous ligand begin to be associated with the globin family [164]. Taking into account the proton donating character of the distal residues and that the *pKa* of free H_2S is around 7, the coordinated sulfide to Fe^{III} would be mainly the monoprotonated species HS^-, or even the deprotonated species S^{2-}, rather than H_2S.

QM calculations of model systems using HS^- coordinated to the heme group revealed that sulfur is negatively charged. Moreover, a few years ago, DFT calculations showed that Fe-bound sulfur behaves as a relatively strong hydrogen bond acceptor on thiolate-bound model porphyrins [165]. MD simulations of Tf-trHbO with coordinated HS^- indicate that only TrpG8 strongly stabilizes the coordinated HS^- through a hydrogen bond interaction, thus accounting for the relatively high affinity for sulfide in these proteins (Fig. 10). When the TrpG8 is mutated to a hydrophobic residue like Phe (both in the single mutant TrpG8F and in the triple mutant TrpG8F-TyrB10F-TyrCD1F), the dissociation constant increases about two orders of magnitude, implying a weakened stabilization of the iron-bound sulfide. This is in agreement with the idea that hydrogen bonding is the main kinetic control of ligand dissociation in heme proteins and confirms the role of TrpG8 in sulfide stabilization in truncated hemoglobins. A similar stabilizing mechanism can be considered for the *L. pectinata* HbI hemoglobin that has the highest affinity for sulfide species among all the heme proteins studied so far [166]. Although it is widely thought that the sulfide species in HbI are stabilized by nearby aromatic residues PheCD1 and PheE11, we instead propose that a hydrogen bond donor, such as GlnE7, is the main stabilizing source for the sulfide ligand, thus playing a similar role as TrpG8 in the trHbOs in maintaining the high affinity for sulfide species.

5. Conclusions

The process of ligand recognition in heme proteins is a complex phenomenon, its description requiring a full understanding of the environment experienced by ligands in heme binding pockets. The present review highlights the contributions of classical, quantum mechanical,

and hybrid quantum-classical computational techniques to the exploration of the molecular basis of ligand binding interactions with globins. In particular, we have shown how structural and conformational features and ligand migration paths can be investigated with classical MD simulations to yield information about free energy barriers and possible secondary docking sites. On the other hand, QM and QM/MM calculations are especially suited to investigate the intrinsic heme reactivity and the protein proximal and distal effects. These two frameworks, classical MD and QM/MM, that cover different time and space scales, complement each other providing a complete picture of the protein function. Computational simulation is a valuable tool often used to validate and contrast experimental observations, and it has been shown to be fully complementary to experimental studies.

Acknowledgements

This work was partially supported by the University of Buenos Aires, Agencia Nacional de Promocion Científica y Tecnológica (project PICT 157), CONICET, European Union Project Nostress, and the Italian Ministero dell'Istruzione, dell'Università e della Ricerca (MIUR), Direzione Generale per l'Internazionalizzazione della Ricerca, Progetti di Grande Rilevanza Italia–Argentina. We thank Mehrnoosh Arrar for close reading and editing of the manuscript.

References

[1] D. Voet, J.G. Voet, Biochemistry, Wiley, 1995.
[2] S.N. Vinogradov, D. Hoogewijs, X. Bailly, R. Arredondo-Peter, J. Gough, S. Dewilde, L. Moens, J.R. Vanfleteren, A phylogenomic profile of globins, BMC Evol. Biol. 6 (2006) 31, (electronic resource).
[3] A. Pesce, M. Bolognesi, A. Bocedi, P. Ascenzi, S. Dewilde, L. Moens, T. Hankeln, T. Burmester, Neuroglobin and cytoglobin. Fresh blood for the vertebrate globin family, EMBO Rep. 3 (2002) 1146–1151.
[4] A. Pesce, M. Couture, S. Dewilde, M. Guertin, K. Yamauchi, P. Ascenzi, L. Moens, M. Bolognesi, A novel two-over-two ?—helical sandwich fold is characteristic of the truncated hemoglobin family, EMBO J. 19 (2000) 2424–2434.
[5] D.A. Vuletich, J.T. Lecomte, A phylogenetic and structural analysis of truncated hemoglobins, J. Mol. Evol. 62 (2006) 196–210.
[6] M. Nardini, A. Pesce, L. Thijs, J.A. Saito, S. Dewilde, M. Alam, P. Ascenzi, M. Coletta, C. Ciacci, L. Moens, M. Bolognesi, Archaeal protoglobin structure indicates new ligand diffusion paths and modulation of haem-reactivity, EMBO Rep. 9 (2008) 157.
[7] M.L. Quillin, R.M. Arduini, J.S. Olson, G.N. Phillips Jr., High-resolution crystal structures of distal histidine mutants of sperm whale myoglobin, J. Mol. Biol. 234 (1993) 140–155.
[8] M. Milani, A. Pesce, Y. Ouellet, P. Ascenzi, M. Guertin, M. Bolognesi, Mycobacterium tuberculosis hemoglobin N displays a protein tunnel suited for O2 diffusion to the heme, EMBO J. 20 (2001) 3902–3909.
[9] M.A. Marti, A. Crespo, L. Capece, L. Boechi, D.E. Bikiel, D.A. Scherlis, D.A. Estrin, Dioxygen affinity in heme proteins investigated by computer simulation, J. Inorg. Biochem. 100 (2006) 761–770.
[10] D.E. Bikiel, L. Boechi, L. Capece, A. Crespo, P.M. De Biase, S. Di Lella, M.C.G. Lebrero, M.A. Marti, A.D. Nadra, L.L. Perissinotti, D.A. Scherlis, D.A. Estrin, Modeling heme proteins using atomistic simulations, Phys. Chem. Chem. Phys. 8 (2006) 5611–5628.
[11] M.A. Marti, L. Capece, A. Bidon-Chanal, A. Crespo, V. Guallar, F.J. Luque, D.A. Estrin, Nitric oxide reactivity with globins as investigated through computer simulation, Methods Enzymol. 437 (2008) 477–498.
[12] P. Arroyo-Manez, D.E. Bikiel, L. Boechi, L. Capece, S. Di Lella, D.A. Estrin, M.A. Marti, D.M. Moreno, A.D. Nadra, A.A. Petruk, Protein dynamics and ligand migration interplay as studied by computer simulation, Biochim. Biophys. Acta 1814 (2011) 1054–1064.
[13] R. Elber, Ligand diffusion in globins: simulations versus experiment, Curr. Opin. Struct. Biol. 20 (2010) 162–167.
[14] M. Laberge, T. Yonetani, Common dynamics of globin family proteins, IUBMB Life 59 (2007) 528–534.
[15] A. Ulitsky, R. Elber, Application of the Locally Enhanced Sampling (LES) and a mean field with a binary collision correction (cLES) to the simulation of Ar diffusion and NO recombination in myoglobin, J. Phys. Chem. 98 (1994) 1034–1043.
[16] J.Z. Ruscio, D. Kumar, M. Shukla, M.G. Prisant, T.M. Murali, A.V. Onufriev, Atomic level computational identification of ligand migration pathways between solvent and binding site in myoglobin, Proc. Natl. Acad. Sci. U. S. A. 105 (2008) 9204–9209.
[17] Y. Nishihara, S. Hayashi, S. Kato, A search for ligand diffusion pathway in myoglobin using a metadynamics simulation, Chem. Phys. Lett. 464 (2008) 220–225.
[18] J. Cohen, A. Arkhipov, R. Braun, K. Schulten, Imaging the migration pathways for O_2, CO, NO, and Xe inside myoglobin, Biophys. J. 91 (2006) 1844–1857.
[19] M. Ceccarelli, R. Anedda, M. Casu, P. Ruggerone, CO escape from myoglobin with metadynamics simulations, Proteins Struct. Funct. Genet. 71 (2008) 1231–1236.
[20] C. Bossa, M. Anselmi, D. Roccatano, A. Amadei, B. Vallone, M. Brunori, A. Di Nola, Extended molecular dynamics simulation of the carbon monoxide migration in sperm whale myoglobin, Biophys. J. 86 (2004) 3855–3862.
[21] A. Bocahut, S. Bernad, P. Sebban, S. Sacquin-Mora, Relating the diffusion of small ligands in human neuroglobin to its structural and mechanical properties, J. Phys. Chem. B 113 (2009) 16257–16267.
[22] D.A. Scherlis, D.A. Estrin, Structure and spin-state energetics of an iron porphyrin model: an assessment of theoretical methods, Int. J. Quantum Chem. 87 (2002) 158–166.
[23] R.J. Deeth, N. Fey, The performance of nonhybrid density functionals for calculating the structures and spin states of Fe(II) and Fe(III) complexes, J. Comput. Chem. 25 (2004) 1840–1848.
[24] T. Yonetani, M. Laberge, Protein dynamics explain the allosteric behaviors of hemoglobin, Biochim. Biophys. Acta Protein Proteomics 1784 (2008) 1146–1158.
[25] L. Mouawad, D. Perahia, C.H. Robert, C. Guilbert, New insights into the allosteric mechanism of human hemoglobin from molecular dynamics simulations, Biophys. J. 82 (2002) 3224–3245.
[26] J.S. Hub, M.B. Kubitzki, B.L. de Groot, Spontaneous quaternary and tertiary T–R transitions of human hemoglobin in molecular dynamics simulation, PLoS Comput. Biol. 6 (2010) 1–11.
[27] S. Fischer, K.W. Olsen, K. Nam, M. Karplus, Unsuspected pathway of the allosteric transition in hemoglobin, Proc. Natl. Acad. Sci. U. S. A. 108 (2011) 5608–5613.
[28] R. Jain, M.K. Chan, Mechanisms of ligand discrimination by heme proteins, J. Biol. Inorg. Chem. 8 (2003) 1–11.
[29] J.S. Olson, G.N. Phillips Jr., Myoglobin discriminates between O_2, NO, and CO by electrostatic interactions with the bound ligand, J. Biol. Inorg. Chem. 2 (1997) 544–552.
[30] L. Capece, M.A. Marti, A. Crespo, F. Doctorovich, D.A. Estrin, Heme protein oxygen affinity regulation exerted by proximal effects, J. Am. Chem. Soc. 128 (2006) 12455–12461.
[31] Q.H. Gibson, R. Regan, R. Elber, J.S. Olson, T.E. Carver, Distal pocket residues affect picosecond ligand recombination in myoglobin. An experimental and molecular dynamics study of position 29 mutants, J. Biol. Chem. 267 (1992) 22022–22034.
[32] P. Arroyo Manez, C. Lu, L. Boechi, M.A. Marti, M. Shepherd, J.L. Wilson, R.K. Poole, F.J. Luque, S.R. Yeh, D.A. Estrin, Role of the distal hydrogen-bonding network in regulating oxygen affinity in the truncated hemoglobin III from *Campylobacter jejuni*, Biochemistry 50 (2011) 3946–3956.
[33] M. Milani, A. Pesce, Y. Ouellet, S. Dewilde, J. Friedman, P. Ascenzi, M. Guertin, M. Bolognesi, Heme-ligand tunneling in group I truncated hemoglobins, J. Biol. Chem. 279 (2004) 21520–21525.
[34] E.E. Scott, Q.H. Gibson, J.S. Olson, Mapping the pathways for O_2 entry into and exit from myoglobin, J. Biol. Chem. 276 (2001) 5177–5188.
[35] S. Franzen, Spin-dependent mechanism for diatomic ligand binding to heme, Proc. Natl. Acad. Sci. U. S. A. 99 (2002) 16754–16759.
[36] A.-L. Tsai, V. Berka, E. Martin, J.S. Olson, A "Sliding Scale Rule" for Selectivity among NO, CO, and O2 by Heme Protein Sensors, Biochemistry 51 (2012) 172–186.
[37] J. Cohen, K.W. Olsen, K. Schulten, K.P. Robert, Finding Gas Migration Pathways in Proteins Using Implicit Ligand Sampling, Methods Enzymol., 437, Academic Press, 2008, pp. 439–457.
[38] O. Carrillo, M. Orozco, GRID-MD—a tool for massive simulation of protein channels, Proteins Struct. Funct. Bioinform. 70 (2008) 892–899.
[39] L. Maragliano, G. Cottone, G. Ciccotti, E. Vanden-Eijnden, Mapping the network of pathways of CO diffusion in myoglobin, J. Am. Chem. Soc. 132 (2010) 1010–1017.
[40] M.S. Shadrina, A.M. English, G.H. Peslherbe, Effective simulations of gas diffusion through kinetically accessible tunnels in multisubunit proteins: O_2 pathways and escape routes in T-state deoxyhemoglobin, J. Am. Chem. Soc. 134 (2012) 11177–11184.
[41] P. Banushkina, M. Meuwly, Free-energy barriers in MbCO rebinding, J. Phys. Chem. B 109 (2005) 16911–16917.
[42] G.M. Torrie, J.P. Valleau, Nonphysical sampling distributions in Monte Carlo free-energy estimation — umbrella sampling, J. Comput. Phys. 23 (1977) 187–199.
[43] X. Wu, S. Wang, Enhancing systematic motion in molecular dynamics simulation, J. Chem. Phys. 110 (1999) 9401–9410.
[44] V. Guallar, C. Lu, K. Borrelli, T. Egawa, S.R. Yeh, Ligand migration in the truncated hemoglobin-II from *Mycobacterium tuberculosis*: the role of G8 tryptophan, J. Biol. Chem. 284 (2009) 3106–3116.
[45] M. Nardini, A. Pesce, M. Milani, M. Bolognesi, Protein fold and structure in the truncated (2/2) globin family, Gene 398 (2007) 2–11.
[46] D. De Sanctis, A. Pesce, M. Nardini, M. Bolognesi, A. Bocedi, P. Ascenzi, Structure–function relationships in the growing hexa-coordinate hemoglobin sub-family, IUBMB Life 56 (2004) 643–651.
[47] T. Egawa, S.R. Yeh, Structural and functional properties of hemoglobins from unicellular organisms as revealed by resonance Raman spectroscopy, J. Inorg. Biochem. 99 (2005) 72–96.
[48] T.G. Spiro, I.H. Wasbotten, CO as a vibrational probe of heme protein active sites, J. Inorg. Biochem. 99 (2005) 34–44.
[49] T.G. Spiro, Biological Applications of Raman Spectroscopy, Wiley, New York, 1988.
[50] D.E. Bikiel, L. Boechi, L. Capece, A. Crespo, P.M. De Biase, S. Di Lella, M.C. Gonzalez Lebrero, M.A. Marti, A.D. Nadra, L.L. Perissinotti, D.A. Scherlis, D.A. Estrin, Modeling heme proteins using atomistic simulations, Phys. Chem. Chem. Phys. 8 (2006) 5611–5628.

[51] C. Rovira, K. Kunc, J. Hutter, P. Ballone, M. Parrinello, Equilibrium geometries and electronic structure of iron–porphyrin complexes: a density functional study, J. Phys. Chem. A 101 (1997) 8914–8925.
[52] H. Lin, D.G. Truhlar, QM/MM: what have we learned, where are we, and where do we go from here? Theoretical chemistry accounts: theory, computation, and modeling, Theoretica Chimica Acta (2006) 185–199.
[53] A. Crespo, D.A. Scherlis, M.A. Marti, P. Ordejón, A.E. Roitberg, D.A. Estrin, A DFT-based QM-MM approach designed for the treatment of large molecular systems: application to chorismate mutase, J. Phys. Chem. B 107 (2003) 13728–13736.
[54] J.W. Ponder, D.A. Case, D. Valerie, Force Fields for Protein Simulations, Adv. Protein Chem., 66, Academic Press, 2003, pp. 27–85.
[55] V. Hornak, R. Abel, A. Okur, B. Strockbine, A. Roitberg, C. Simmerling, Comparison of multiple amber force fields and development of improved protein backbone parameters, Proteins Struct. Funct. Genet. 65 (2006) 712–725.
[56] A.D. MacKerell Jr., B. Brooks, C.L. Brooks III, L. Nilsson, B. Roux, Y. Won, M. Karplus, CHARMM: the Energy Function and Its Parameterization With an Overview of the Program, in: J.W. Sons (Ed.), The Encyclopedia of Computational Chemistry, 1998, pp. 271–277.
[57] J.M. Wang, P. Cieplak, P.A. Kollman, How well does a restrained electrostatic potential (RESP) model perform in calculating conformational energies of organic and biological molecules? J. Comput. Chem. 21 (2000) 1049–1074.
[58] F.P. Nicoletti, E. Droghetti, L. Boechi, A. Bonamore, N. Sciamanna, D.A. Estrin, A. Feis, A. Boffi, G. Smulevich, Fluoride as a probe for H-bonding interactions in the active site of heme proteins: the case of *Thermobifida fusca* hemoglobin, J. Am. Chem. Soc. 133 (2011) 20970–20980.
[59] F.P. Nicoletti, A. Comandini, A. Bonamore, L. Boechi, F.M. Boubeta, A. Feis, G. Smulevich, A. Boffi, Sulfide binding properties of truncated hemoglobins, Biochemistry 49 (2010) 2269–2278.
[60] L.L. Perissinotti, M.A. Marti, F. Doctorovich, F.J. Luque, D.A. Estrin, A microscopic study of the deoxyhemoglobin-catalyzed generation of nitric oxide from nitrite anion, Biochemistry 47 (2008) 9793–9802.
[61] L. Boechi, M.A. Marti, A. Vergara, F. Sica, L. Mazzarella, D.A. Estrin, A. Merlino, Protonation of histidine 55 affects the oxygen access to heme in the alpha chain of the hemoglobin from the Antarctic fish *Trematomus bernacchii*, IUBMB Life 63 (2011) 175–182.
[62] J. Kästner, Umbrella sampling, WIREs Comput. Mol. Sci. 1 (2011) 932–942.
[63] A. Laio, M. Parrinello, Escaping free-energy minima, Proc. Natl. Acad. Sci. U. S. A. 99 (2002) 12562–12566.
[64] K.W. Borrelli, A. Vitalis, R. Alcantara, V. Guallar, PELE: Protein Energy Landscape Exploration. A novel Monte Carlo based technique, J. Chem. Theory Comput. 1 (2005) 1304–1311.
[65] M.F. Lucas, V. Guallar, An atomistic view on human hemoglobin carbon monoxide migration processes, Biophys. J. 102 (2012) 887–896.
[66] F. Forti, L. Boechi, D.A. Estrin, M.A. Marti, Comparing and combining implicit ligand sampling with multiple steered molecular dynamics to study ligand migration processes in heme proteins, J. Comput. Chem. 32 (2011) 2219–2231.
[67] M. Milani, A. Pesce, M. Nardini, H. Ouellet, Y. Ouellet, S. Dewilde, A. Bocedi, P. Ascenzi, M. Guertin, L. Moens, J.M. Friedman, J.B. Wittenberg, M. Bolognesi, Structural bases for heme binding and diatomic ligand recognition in truncated hemoglobins, J. Inorg. Biochem. 99 (2005) 97–109.
[68] Y.H. Ouellet, R. Daigle, P. Lague, D. Dantsker, M. Milani, M. Bolognesi, J.M. Friedman, M. Guertin, Ligand binding to truncated hemoglobin N from *Mycobacterium tuberculosis* is strongly modulated by the interplay between the distal heme pocket residues and internal water, J. Biol. Chem. 283 (2008) 27270–27278.
[69] R.A. Goldbeck, S. Bhaskaran, C. Ortega, J.L. Mendoza, J.S. Olson, J. Soman, D.S. Kliger, R.M. Esquerra, Water and ligand entry in myoglobin: assessing the speed and extent of heme pocket hydration after CO photodissociation, Proc. Natl. Acad. Sci. U. S. A. 103 (2006) 1254–1259.
[70] M.F. Perutz, F.S. Mathews, An X-ray study of azide methaemoglobin, J. Mol. Biol. 21 (1966) 199–202.
[71] J.S. Olson, J. Soman, G.N. Phillips Jr., Ligand pathways in myoglobin: a review of Trp cavity mutations, IUBMB Life 59 (2007) 552–562.
[72] F. Yang, G.N. Phillips Jr., Crystal structures of CO-, Deoxy- and Met-myoglobins at various pH values, J. Mol. Biol. 256 (1996) 762–774.
[73] W.D. Tian, J.T. Sage, P.M. Champion, Investigations of ligand association and dissociation rates in the “open” and “closed” states of myoglobin, J. Mol. Biol. 233 (1993) 155–166.
[74] L. Boechi, M. Arrar, M.A. Marti, J. Olson, A. Roitberg, D.A. Estrin, Hydrophobic effect drives oxygen uptake in myoglobin via histidine E7, J. Biol. Chem. 288 (2013) 6754–6762.
[75] M. Brunori, Q.H. Gibson, Cavities and packing defects in the structural dynamics of myoglobin, EMBO Rep. 2 (2001) 674–679.
[76] D. Bourgeois, B. Vallone, F. Schotte, A. Arcovito, A.E. Miele, G. Sciara, M. Wulff, P. Anfinrud, M. Brunori, Complex landscape of protein structural dynamics unveiled by nanosecond Laue crystallography, Proc. Natl. Acad. Sci. U. S. A. 100 (2003) 8704–8709.
[77] A. Crespo, M.A. Marti, S.G. Kalko, A. Morreale, M. Orozco, J.L. Gelpi, F.J. Luque, D.A. Estrin, Theoretical study of the truncated hemoglobin HbN: exploring the molecular basis of the NO detoxification mechanism, J. Am. Chem. Soc. 127 (2005) 4433–4444.
[78] A. Bidon-Chanal, M.A. Marti, A. Crespo, M. Milani, M. Orozco, M. Bolognesi, F.J. Luque, D.A. Estrin, Ligand-induced dynamical regulation of NO conversion in *Mycobacterium tuberculosis* truncated hemoglobin-N, Proteins Struct. Funct. Bioinform. 64 (2006) 457–464.
[79] A. Bidon-Chanal, M.A. Marti, D.A. Estrin, F.J. Luque, Dynamical regulation of ligand migration by a gate-opening molecular switch in truncated hemoglobin-N from *Mycobacterium tuberculosis*, J. Am. Chem. Soc. 129 (2007) 6782.
[80] L. Giangiacomo, A. Ilari, A. Boffi, V. Morea, E. Chiancone, The truncated oxygen-avid hemoglobin from Bacillus subtilis: X-ray structure and ligand binding properties, J. Biol. Chem. 280 (2005) 9192–9202.
[81] L. Boechi, P.A. Manez, F.J. Luque, M.A. Marti, D.A. Estrin, Unraveling the molecular basis for ligand binding in truncated hemoglobins: the trHbO *Bacillus subtilis* case, Proteins 78 (2010) 962–970.
[82] Y. Ouellet, M. Milani, M. Couture, M. Bolognesi, M. Guertin, Ligand interactions in the distal heme pocket of *Mycobacterium tuberculosis* truncated hemoglobin N: roles of TyrB10 and GlnE11 residues, Biochemistry 45 (2006) 8770–8781.
[83] L. Boechi, M.A. Marti, M. Milani, M. Bolognesi, F.J. Luque, D.A. Estrin, Structural determinants of ligand migration in *Mycobacterium tuberculosis* truncated hemoglobin O, Proteins 73 (2008) 372–379.
[84] M.A. Marti, A. Bidon-Chanal, A. Crespo, S.-R. Yeh, V. Guallar, F.J. Luque, D.A. Estrin, Mechanism of product release in NO detoxification from *Mycobacterium tuberculosis* truncated hemoglobin N, J. Am. Chem. Soc. 130 (2008) 1688–1693.
[85] B. Roux, S. Berneche, B. Egwolf, B. Lev, S.Y. Noskov, C.N. Rowley, H. Yu, Ion selectivity in channels and transporters, J. Gen. Physiol. 137 (2011) 415–426.
[86] H. Ouellet, L. Juszczak, D. Dantsker, U. Samuni, Y.H. Ouellet, P.Y. Savard, J.B. Wittenberg, B.A. Wittenberg, J.M. Friedman, M. Guertin, Reactions of *Mycobacterium tuberculosis* truncated hemoglobin O with ligands reveal a novel ligand-inclusive hydrogen bond network, Biochemistry 42 (2003) 5764–5774.
[87] M.A. Marti, D.E. Bikiel, A. Crespo, M. Nardini, M. Bolognesi, D.A. Estrin, Two distinct heme distal site states define *Cerebratulus lacteus* mini-hemoglobin oxygen affinity, Proteins Struct. Funct. Bioinform. 62 (2006) 641–648.
[88] A. Pesce, M. Nardini, P. Ascenzi, E. Geuens, S. Dewilde, L. Moens, M. Bolognesi, A.F. Riggs, A. Hale, P. Deng, G.U. Nienhaus, J.S. Olson, K. Nienhaus, Thr-E11 regulates O2 affinity in *Cerebratulus lacteus* mini-hemoglobin, J. Biol. Chem. 279 (2004) 33662–33672.
[89] M.A. Marti, L. Capece, D.E. Bikiel, B. Falcone, D.A. Estrin, Oxygen affinity controlled by dynamical distal conformations: the soybean leghemoglobin and the *Paramecium caudatum* hemoglobin cases, Proteins 68 (2007) 480–487.
[90] S. Kundu, G.C. Blouin, S.A. Premer, G. Sarath, J.S. Olson, M.S. Hargrove, Tyrosine B10 inhibits stabilization of bound carbon monoxide and oxygen in soybean leghemoglobin, Biochemistry 43 (2004) 6241–6252.
[91] S. Kundu, J.T. Trent Iii, M.S. Hargrove, Plants, humans and hemoglobins, Trends Plant Sci. 8 (2003) 387–393.
[92] C. Lu, T. Egawa, L.M. Wainwright, R.K. Poole, S.R. Yeh, Structural and functional properties of a truncated hemoglobin from a food-borne pathogen *Campylobacter jejuni*, J. Biol. Chem. 282 (2007) 13627–13636.
[93] A. Bonamore, A. Boffi, Flavohemoglobin: structure and reactivity, IUBMB Life 60 (2008) 19–28.
[94] A. Ilari, A. Boffi, Structural studies on flavohemoglobins, Methods Enzymol. 436 (2008) 187–202.
[95] A.M. Gardner, P.R. Gardner, Flavohemoglobin detoxifies nitric oxide in aerobic, but not anaerobic, *Escherichia coli*. Evidence for a novel inducible anaerobic nitric oxide-scavenging activity, J. Biol. Chem. 277 (2002) 8166–8171.
[96] H. Ouellet, Y. Ouellet, C. Richard, M. Labarre, B. Wittenberg, J. Wittenberg, M. Guertin, Truncated hemoglobin HbN protects *Mycobacterium* bovis from nitric oxide, Proc. Natl. Acad. Sci. U. S. A. 99 (2002) 5902–5907.
[97] D.N. Ferreiro, L. Boechi, D.A. Estrin, M.A. Marti, The key role of water in the dioxygenase function of *Escherichia coli* flavohemoglobin, J. Inorg. Biochem. 119C (2012) 75–84.
[98] S. Kundu, B. Snyder, K. Das, P. Chowdhury, J. Park, J.W. Petrich, M.S. Hargrove, The leghemoglobin proximal heme pocket directs oxygen dissociation and stabilizes bound heme, Proteins Struct. Funct. Genet. 46 (2002) 268–277.
[99] T.K. Das, R.E. Weber, S. Dewilde, J.B. Wittenberg, B.A. Wittenberg, K. Yamauchi, M.L. Van Hauwaert, L. Moens, D.L. Rousseau, Ligand binding in the ferric and ferrous states of *Paramecium* hemoglobin, Biochemistry 39 (2000) 14330–14340.
[100] A.M. Gardner, L.A. Martin, P.R. Gardner, Y. Dou, J.S. Olson, Steady-state and transient kinetics of *Escherichia coli* nitric-oxide dioxygenase (flavohemoglobin). The B10 tyrosine hydroxyl is essential for dioxygen binding and catalysis, J. Biol. Chem. 275 (2000) 12581–12589.
[101] P.R. Gardner, A.M. Gardner, L.A. Martin, Y. Dou, T. Li, J.S. Olson, H. Zhu, A.F. Riggs, Nitric-oxide dioxygenase activity and function of flavohemoglobins. sensitivity to nitric oxide and carbon monoxide inhibition, J. Biol. Chem. 275 (2000) 31581–31587.
[102] D.E. Bikiel, F. Forti, L. Boechi, M. Nardini, F.J. Luque, M.A. MartiÃÅ, D.A. Estrin, Role of heme distortion on oxygen affinity in heme proteins: the protoglobin case, J. Phys. Chem. B 114 (2010) 8536–8543.
[103] D.B. Goodin, D.E. McRee, The Asp–His–Fe triad of cytochrome c peroxidase controls the reduction potential, electronic structure, and coupling of the tryptophan free radical to the heme, Biochemistry 32 (1993) 3313–3324.
[104] K.M. Vogel, P.M. Kozlowski, M.Z. Zgierski, T.G. Spiro, Determinants of the FeXo (X = C, N, O) vibrational frequencies in heme adducts from experiment and density functional theory, J. Am. Chem. Soc. 121 (1999) 9915–9921.
[105] W.A. Oertling, R. Hille, Resonance-enhanced Raman scattering from the molybdenum center of xanthine oxidase, J. Biol. Chem. 265 (1990) 17446–17450.
[106] M.S. Hargrove, J.K. Barry, E.A. Brucker, M.B. Berry, G.N. Phillips Jr., J.S. Olson, R. Arredondo-Peter, J.M. Dean, R.V. Klucas, G. Sarath, Characterization of recombinant soybean leghemoglobin a and apolar distal histidine mutants, J. Mol. Biol. 266 (1997) 1032–1042.
[107] W.A. Eaton, E.R. Henry, J. Hofrichter, S. Bettati, C. Viappiani, A. Mozzarelli, Evolution of allosteric models for hemoglobin, IUBMB Life 59 (2007) 586–599.

[108] M.F. Perutz, G. Fermi, B. Luisi, B. Shaanan, R.C. Liddington, Stereochemistry of cooperative mechanisms in hemoglobin, Acc. Chem. Res. 20 (1987) 309–321.
[109] D.E. Bikiel, S.E. Bari, F.A. Doctorovich, D.A. Estrin, DFT study on the reactivity of iron porphyrins tuned by ring substitution J, J. Inorg. Biochem. 102 (2008) 70–76.
[110] N.W. Alcock, T.J. Kemp, T.K. Chandrashekar, R.J. Deeth, J. Leciejewicz, H.D. Lutz, M. Ravikanth, Coordination Chemistry, Springer Verlag, 1995.
[111] W. Jentzen, M.C. Simpson, J.D. Hobbs, X. Song, T. Ema, N.Y. Nelson, C.J. Medforth, K.M. Smith, M. Veyrat, M. Mazzanti, R. Ramasseul, J.C. Marchon, T. Takeuchi, W.A. Goddard Iii, J.A. Shelnutt, Ruffling in a series of nickel(II) mesco-tetrasubstituted porphyrins as a model for the conserved ruffling of the heme of cytochromes c, J. Am. Chem. Soc. 117 (1995) 11085–11097.
[112] J.A. Shelnutt, X.Z. Song, J.G. Ma, S.L. Jia, W. Jentzen, C.J. Medforth, Nonplanar porphyrins and their significance in proteins, Chem. Soc. Rev. 27 (1998) 31–41.
[113] W. Jentzen, X.Z. Song, J.A. Shelnutt, Structural characterization of synthetic and protein-bound porphyrins in terms of the lowest-frequency normal coordinates of the macrocycle, J. Phys. Chem. B 101 (1997) 1684–1699.
[114] B.D. Howes, C.B. Schiodt, K.G. Welinder, M.P. Marzocchi, J.G. Ma, J. Zhang, J.A. Shelnutt, G. Smulevich, The quantum mixed-spin heme state of barley peroxidase: a paradigm for class III peroxidases, Biophys. J. 77 (1999) 478–492.
[115] J.A. Shelnutt, The Porphyrins Handbook, in: C.M. Kadish, K.M. Smith, R. Guilard (Eds.), The Porphyrins Handbook, Academic Press, San Diego, 2000, pp. 167–223.
[116] S.A. Roberts, A. Weichsel, Y. Qiu, J.A. Shelnutt, F.A. Walker, W.R. Montfort, Biochemistry 40 (2001) 11327.
[117] T.K. Shokhireva, R.E. Berry, E. Uno, C.A. Balfour, H. Zhang, F.A. Walker, Proc. Natl. Acad. Sci. U. S. A. 100 (2003) 3778.
[118] E.M. Maes, S.A. Roberts, A. Weichsel, W.R. Montfort, Biochemistry 44 (2005) 12690.
[119] K.M. Barkigia, M. Palacio, Y. Sun, M. Nogues, M.W. Renner, F. Varret, P. Battioni, D. Mansuy, F. Fajer, Inorg. Chem. 41 (2002) 5647.
[120] A.A. Jarzecki, T.G. Spiro, J. Phys. Chem. A 109 (2005) 421.
[121] S. Venkateshrao, J. Yin, A.A. Jarzecki, P.G. Schultz, T.G. Spiro, J. Am. Chem. Soc. 126 (2004) 16361.
[122] A. Feis, A. Lapini, B. Catacchio, S. Brogioni, P. Foggi, E. Chiancone, A. Boffi, G. Smulevich, Unusually strong H-bonding to the heme ligand and fast geminate recombination dynamics of the carbon monoxide complex of *Bacillus subtilis* truncated hemoglobin, Biochemistry 47 (2007) 902–910.
[123] E. Droghetti, F.P. Nicoletti, A. Bonamore, L. Boechi, P. Arroyo Manez, D.A. Estrin, A. Boffi, G. Smulevich, A. Feis, Heme pocket structural properties of a bacterial truncated hemoglobin from *Thermobifida fusca*, Biochemistry 49 (2010) 10394–10402.
[124] M. Mukai, C.E. Mills, R.K. Poole, S.R. Yeh, Flavohemoglobin, a globin with a peroxidase-like catalytic site, J. Biol. Chem. 276 (2001) 7272–7277.
[125] L. Ye, D. Spiteller, R. Ullrich, W. Boland, J. Nuske, G. Diekert, Fluoride-dependent conversion of organic compounds mediated by manganese peroxidases in the absence of Mn(2+) ions, Biochemistry 49 (2010) 7264–7271.
[126] E. Droghetti, F.P. Nicoletti, A. Bonamore, N. Sciamanna, A. Boffi, A. Feis, G. Smulevich, The optical spectra of fluoride complexes can effectively probe H-bonding interactions in the distal cavity of heme proteins, J. Inorg. Biochem. 105 (2011) 1338–1343.
[127] F. Neri, D. Kok, M.A. Miller, G. Smulevich, Fluoride binding in hemoproteins: the importance of the distal cavity structure, Biochemistry 36 (1997) 8947–8953.
[128] D.E. Koshland Jr., The dimensions of the brain, Science 258 (1992) 199.
[129] M.A. Marletta, Nitric oxide synthase: aspects concerning structure and catalysis, Cell 78 (1994) 927–930.
[130] T.G. Traylor, V.S. Sharma, Why NO? Biochemistry 31 (1992) 2847–2849.
[131] J.R. Stone, M.A. Marletta, Spectral and kinetic studies on the activation of soluble guanylate cyclase by nitric oxide, Biochemistry 35 (1996) 1093–1099.
[132] M.A. Marti, D.A. Scherlis, F.A. Doctorovich, P. Ordejón, D.A. Estrin, Modulation of the NO trans effect in heme proteins: Implications for the activation of soluble guanylate cyclase, J. Biol. Inorg. Chem. 8 (2003) 595–600.
[133] C.R. Andrew, E.L. Green, D.M. Lawson, R.R. Eady, Resonance Raman studies of cytochrome c′ support the binding of NO and CO to opposite sides of the heme: implications for ligand discrimination in heme-based sensors, Biochemistry 40 (2001) 4115–4122.
[134] M.A. Marti, L. Capece, A. Crespo, F. Doctorovich, D.A. Estrin, Nitric oxide interaction with cytochrome c? and its relevance to guanylate cyclase. Why does the iron histidine bond break? J. Am. Chem. Soc. 127 (2005) 7721–7728.
[135] P. Lumme, J. Tummavuo, Potentiometric Determination of Ionization Constant of Nitrous Acid in Aqueous Sodium Perchlorate Solutions at 25 Degrees C, Acta Chem. Scand. 19 (1965) 617–621.
[136] P.A. Williams, V. Fulop, E.F. Carman, N.F.W. Saunders, S.J. Ferguson, J. Hajdu, Haem-ligand switching during catalysis in crystals of a nitrogen-cycle enzyme, Nature 389 (1997) 406–412.
[137] M.A. Marti, A. Crespo, S.E. Bari, F.A. Doctorovich, D.A. Estrin, QM-MM Study of Nitrite Reduction by Nitrite Reductase of Pseudomonas aeruginosa, J. Phys. Chem. B 108 (2004) 18073–18080.
[138] G. Ranghino, E. Scorza, T. Sjogren, P.A. Williams, M. Ricci, J. Hajdu, Quantum mechanical interpretation of nitrite reduction by cytochrome cd1 nitrite reductase from Paracoccus pantotrophus, Biochemistry 39 (2000) 10958–10966.
[139] S. Rinaldo, A. Arcovito, M. Brunori, F. Cutruzzola, Fast dissociation of nitric oxide from ferrous Pseudomonas aeruginosa cd1 nitrite reductase. A novel outlook on the catalytic mechanism, J. Biol. Chem. 282 (2007) 14761–14767.
[140] B.A. Averill, Dissimilatory Nitrite and Nitric Oxide Reductases, Chem. Rev. 96 (1996) 2951–2964.
[141] M.T. Gladwin, A.N. Schechter, NO contest — Nitrite versus S-nitroso-hemoglobin, Circ. Res. 94 (2004) 851–855.
[142] K. Cosby, K.S. Partovi, J.H. Crawford, R.P. Patel, C.D. Reiter, S. Martyr, B.K. Yang, M.A. Waclawiw, G. Zalos, X. Xu, K.T. Huang, H. Shields, D.B. Kim-Shapiro, A.N. Schechter, R.O. Cannon Iii, M.T. Gladwin, Nitrite reduction to nitric oxide by deoxyhemoglobin vasodilates the human circulation, Nat. Med. 9 (2003) 1498–1505.
[143] D.B. Kim-Shapiro, M.T. Gladwin, R.P. Patel, N. Hogg, The reaction between nitrite and hemoglobin: the role of nitrite in hemoglobin-mediated hypoxic vasodilation, J. Inorg. Biochem. 99 (2005) 237–246.
[144] K.T. Huang, A. Keszler, N. Patel, R.P. Patel, M.T. Gladwin, D.B. Kim-Shapiro, N. Hogg, The reaction between nitrite and deoxyhemoglobin. Reassessment of reaction kinetics and stoichiometry, J. Biol. Chem. 280 (2005) 31126–31131.
[145] Z. Huang, S. Shiva, D.B. Kim-Shapiro, R.P. Patel, L.A. Ringwood, C.E. Irby, K.T. Huang, C. Ho, N. Hogg, A.N. Schechter, M.T. Gladwin, Enzymatic function of hemoglobin as a nitrite reductase that produces NO under allosteric control, J. Clin. Invest. 115 (2005) 2099–2107.
[146] U.B. Hendgen-Cotta, M.W. Merx, S. Shiva, J. Schmitz, S. Becher, J.P. Klare, H.J. Steinhoff, A. Goedecke, J. Schrader, M.T. Gladwin, M. Kelm, T. Rassaf, Nitrite reductase activity of myoglobin regulates respiration and cellular viability in myocardial ischemia-reperfusion injury, Proc. Natl. Acad. Sci. U. S. A. 105 (2008) 10256–10261.
[147] M. Totzeck, U.B. Hendgen-Cotta, P. Luedike, M. Berenbrink, J.P. Klare, H.J. Steinhoff, D. Semmler, S. Shiva, D. Williams, A. Kipar, M.T. Gladwin, J. Schrader, M. Kelm, A.R. Cossins, T. Rassaf, Nitrite regulates hypoxic vasodilation via myoglobin-dependent nitric oxide generation, Circulation 126 (2012) 325–334.
[148] S.J. George, J.W. Allen, S.J. Ferguson, R.N. Thorneley, Time-resolved infrared spectroscopy reveals a stable ferric heme-NO intermediate in the reaction of Paracoccus pantotrophus cytochrome cd1 nitrite reductase with nitrite, J. Biol. Chem. 275 (2000) 33231–33237.
[149] F. Cutruzzola, K. Brown, E.K. Wilson, A. Bellelli, M. Arese, M. Tegoni, C. Cambillau, M. Brunori, The nitrite reductase from Pseudomonas aeruginosa: Essential role of two active-site histidines in the catalytic and structural properties, Proc. Natl. Acad. Sci. U. S. A. 98 (2001) 2232–2237.
[150] R. Silaghi-Dumitrescu, Linkage isomerism in nitrite reduction by cytochrome cd(1) nitrite reductase, Inorg. Chem. 43 (2004) 3715–3718.
[151] S. Basu, R. Grubina, J. Huang, J. Conradie, Z. Huang, A. Jeffers, A. Jiang, X. He, I. Azarov, R. Seibert, A. Mehta, R. Patel, S.B. King, N. Hogg, A. Ghosh, M.T. Gladwin, D.B. Kim-Shapiro, Catalytic generation of N2O3 by the concerted nitrite reductase and anhydrase activity of hemoglobin, Nat. Chem. Biol. 3 (2007) 785–794.
[152] M.S. Navati, J.M. Friedman, Reactivity of glass-embedded met hemoglobin derivatives toward external NO: implications for nitrite-mediated production of bioactive NO, J. Am. Chem. Soc. 131 (2009) 12273–12279.
[153] G.R. Wyllie, W.R. Scheidt, Solid-state structures of metalloporphyrin NO(x)compounds, Chem. Rev. 102 (2002) 1067–1090.
[154] I.V. Novozhilova, P. Coppens, J. Lee, G.B. Richter-Addo, K.A. Bagley, Experimental and density functional theoretical investigations of linkage isomerism in six-coordinate FeNO(6) iron porphyrins with axial nitrosyl and nitro ligands, J. Am. Chem. Soc. 128 (2006) 2093–2104.
[155] H. Nasri, M.K. Ellison, M. Shang, C.E. Schulz, W.R. Scheidt, Variable pi-bonding in iron(II) porphyrinates with nitrite, CO, and tert-butyl isocyanide: characterization of [Fe(TpivPP)(NO2)(CO)], Inorg. Chem. 43 (2004) 2932–2942.
[156] J. Lee, A.Y. Kovalevsky, I.V. Novozhilova, K.A. Bagley, P. Coppens, G.B. Richter-Addo, Single- and double-linkage isomerism in a six-coordinate iron porphyrin containing nitrosyl and nitro ligands, J. Am. Chem. Soc. 126 (2004) 7180–7181.
[157] O. Einsle, A. Messerschmidt, R. Huber, P.M. Kroneck, F. Neese, Mechanism of the six-electron reduction of nitrite to ammonia by cytochrome c nitrite reductase, J. Am. Chem. Soc. 124 (2002) 11737–11745.
[158] B.R. Crane, L.M. Siegel, E.D. Getzoff, Probing the catalytic mechanism of sulfite reductase by X-ray crystallography: structures of the Escherichia coli hemoprotein in complex with substrates, inhibitors, intermediates, and products, Biochemistry 36 (1997) 12120–12137.
[159] D.M. Copeland, A.S. Soares, A.H. West, G.B. Richter-Addo, Crystal structures of the nitrite and nitric oxide complexes of horse heart myoglobin, J. Inorg. Biochem. 100 (2006) 1413–1425.
[160] J. Yi, J. Heinecke, H. Tan, P.C. Ford, G.B. Richter-Addo, The distal pocket histidine residue in horse heart myoglobin directs the O-binding mode of nitrite to the heme iron, J. Am. Chem. Soc. 131 (2009) 18119–18128.
[161] J. Yi, M.K. Safo, G.B. Richter-Addo, The Nitrite Anion Binds to Human Hemoglobin via the Uncommon O-Nitrito Mode, Biochemistry 47 (2008) 8247–8249.
[162] Y.W. Lin, C.M. Nie, L.F. Liao, Rational design of a nitrite reductase based on myoglobin: a molecular modeling and dynamics simulation study, J. Mol. Model. 18 (2012) 4409–4415.
[163] D.W. Kraus, J.B. Wittenberg, Hemoglobins of the Lucina pectinata/bacteria symbiosis. I. Molecular properties, kinetics and equilibria of reactions with ligands, J. Biol. Chem. 265 (1990) 16043–16053.
[164] X. Bailly, S. Vinogradov, The sulfide binding function of annelid hemoglobins: relic of an old biosystem? J. Inorg. Biochem. 99 (2005) 142–150.
[165] A. Dey, T.A. Okamura, N. Ueyama, B. Hedman, K.O. Hodgson, E.I. Solomon, Sulfur K-edge XAS and DFT calculations on P450 model complexes: effects of hydrogen bonding on electronic structure and redox potentials, J. Am. Chem. Soc. 127 (2005) 12046–12053.
[166] R. Pietri, A. Lewis, R.G. Leon, G. Casabona, L. Kiger, S.R. Yeh, S. Fernandez-Alberti, M.C. Marden, C.L. Cadilla, J. Lopez-Garriga, Factors controlling the reactivity of hydrogen sulfide with hemeproteins, Biochemistry 48 (2009) 4881–4894.